Final Report
September, 2008

Research and development of a new field enhanced low temperature thermionic cathode that enables fluorescent dimming and load shedding without auxiliary cathode heating

Work Performed Under Agreement:
DE-FC26-04NT-42329

Submitted by:
Ball State University
Muncie, IN 46308

Principal Investor:
Feng Jin
Phone: 765-285-3747
E-mail: fjin@bsu.edu

Submitted to:
US department of Energy
National Energy Technology Laboratory

Contract Specialist: Sue Miltenberger
E-Mail: Susan.Miltenberger@netl.doe.gov

COR: Joel S. Chaddock
E-Mail: Joel.Chaddock@NETL.DOE.GOV

DISCLAIMER

Table of Contents

Summary ……2

A. Project Background ……3

B. CNT Growth ……..…..…….5

C. Oxide Deposition and Prototype Cathode Development …….16

D. Electron Emission Measurement Techniques and Characterizations of Emission of Prototype Cathode in Vacuum ……..35

E. Thermionic Cooling Phenomenon ……...40

F. Discharge Simulator and Prototype Performance in Plasma ……...45

Conclusions ……..53

Appendix A: List of the publications under the project ……. 54

Summary

This is the final report for project entitled “Research and development of a new field enhanced low temperature thermionic cathode that enables fluorescent dimming and load shedding without auxiliary cathode heating”, under Agreement Number: DE-FC26-04NT-42329. Under this project, a highly efficient CNT based thermionic cathode was demonstrated. This cathode is capable of emitting electron at a current density two order of magnitude stronger then a typical fluorescent cathode at same temperatures, or capable of emitting at same current density but at temperature about 300 ^{o}C lower than that of a fluorescent cathode. Detailed fabrication techniques were developed including CVD growth of CNTs and sputter deposition of oxide thin films on CNTs. These are mature technologies that have been widely used in industry for large scale materials processing and device fabrications, thus, with further development work, the techniques developed in this project can be scaled-up in manufacturing environment. The prototype cathodes developed in this project were tested in lighting plasma discharge environment. In many cases, they not only lit and sustain the plasma, but also out perform the fluorescent cathodes in key parameters such like cathode fall voltages. More work will be needed to further evaluate more detailed and longer term performance of the prototype cathode in lighting plasma.

A. Project Background

Dimming is an effective way to reduce the energy consumption of fluorescent systems. However, current dimming technology suffers from high dimming ballast cost, shortened lamp life and to a lesser degree, relatively low ballast and lamp efficiency. These major issues prevent broad market acceptance of the dimming technology. Currently the dimming ballast market share in the US is only 1% of the total ballast market. The cause for these problems is that current fluorescent dimming systems require rather sophisticated and expensive auxiliary cathode heating to maintain the temperature of a fluorescent cathode to its thermionic emission temperature. It is the goal of this research to explore a cathode technology that will eliminate the need for auxiliary cathode heating for dimming.

The objective of this research is to develop a new type of low temperature thermionic cathodes that are capable of emitting sufficient electron current at a much lower temperature, and thus to eliminate the need for auxiliary cathode heating for fluorescent dimming systems.

With the current cathode technology, when dimming, an auxiliary cathode heating is needed because the reduced lamp current alone cannot keep the cathode to its thermionic emission temperature. Without this auxiliary cathode heating, the lamp cathode would be too "cool" to supply the needed electron current in the dimming operation mode. Consequently, the cathode fall voltage, a high voltage in front of the sheath of the cathode, will increase to generate a large amount of ion current to make up the loss of electron current. This ion current, coupled with high cathode fall voltage, will cause sputtering damage to the cathode and shorten the lamp life. This auxiliary cathode heating, while needed in the dimming mode, can also overheat the cathode and cause excess evaporation of emission materials and shorten the lamp life. For that reason, current dimming ballasts employ various methods to control auxiliary cathode heating as a function of lamp current or level of dimming. The designs and circuits for the dimming ballasts are much more complex than the instant start ballasts, which don't have auxiliary cathode heating. As a result, the dimming ballasts have much higher costs and significantly lower ballast efficiency compared to instant start ballasts. Furthermore, even with rather sophisticated designs and costly circuits, because of the complexity of interaction between lamp current and auxiliary cathode heating, the performances of dimming systems installed are not always satisfactory; often times they resulted in shortening the lamp life.

The basic idea of this project is to develop a fluorescent cathode that is capable of emitting enough electron current for lamp operation even at a much lower temperature, i.e. under reduced lamp current in dimming conditions, so that auxiliary heating wouldn't be needed any more, and thus eliminate the source of all the problems associated with dimming. We have developed the idea of a field enhanced thermionic cathode and conducted preliminary research to demonstrate the concept and feasibility.

The uniqueness of this cathode, as illustrated in Figure 1, is that it utilizes carbon nanotubes to induce a significant field enhanced effect in thermionic electron emission. The main feature of this cathode is that it consists of carbon nanotubes with a surface coating of thermionic materials; thus it combines CNT's unique geometry with the electron emission property of thermionic materials, and utilizes the field enhancement effect from carbon nanotubes to enhance the cathode's thermionic electron emission.

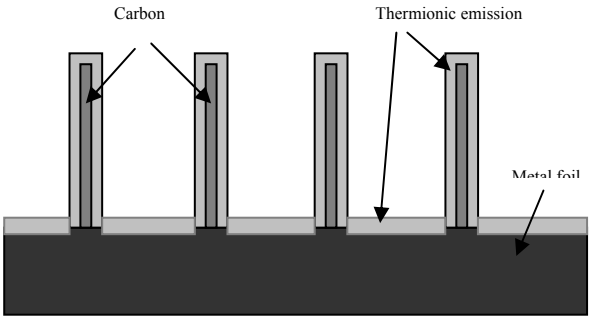

Figure 1. A schematic of the proposed cathode

The field emission in traditional fluorescent cathodes is insignificant. The thermionic emission from a fluorescent cathode is given by the Richardson-Dushman equation:

$$J_s = 120T^2 e^{\frac{-11{,}605\varphi}{T}} e^{\frac{4.4\sqrt{E}}{T}} \qquad (1)$$

where T is temperature, ϕ is work function, E in this term is the external electrical field in volts/cm, and the last exponential term is the field enhancement due to the Schottky effect. Fluorescent cathodes are coated with low work function emission materials, usually barium rich oxides, and operate at above 1000 ^{0}C to enhance thermionic electron emission. Although the cathode fall in a fluorescent lamp is approximately 15 V, the sheath thickness in front of a fluorescent cathode is very thin and is typically in the order of 10 μm. This results in a rather large electric field of approximately 10^4 V/cm, or 1 V/μm. But even with this large field, the effect of field enhancement in thermionic emission from a fluorescent cathode is not very significant. For instance, we can calculate that the field enhanced thermionic emission would be only 1.5 times the zero-field emission with a large external electric field of 1 V/μm. A small increase in the external field does not lead to significant improvement in thermionic emission. For that reason, field enhanced thermionic emission has never been extensively explored and there are no reported studies on this subject in the literature except our recent report.

However, with the introduction of carbon nanotubes, our new cathode will have a strong field enhanced electron emission. The unique geometry and high aspect ratio of carbon nanotubes give rise to a large local field enhancement factor. Field enhancement factors as high as 10,000 times have been reported in CNT field emitter

studies in the literature. Coupled with thermionic emission from oxide emissive coating, this new cathode will be capable of emitting sufficient electron current required for sustaining lamp operation at a much lower temperature.

In our case, assuming that we can eventually manage to achieve a modest local field enhancement factor of 300, or $F = 10^4 \times 300 = 3 \times 10^6$ V/cm, the field enhanced thermionic emission will be 2,040 times the zero field emission, or 2040/1.5 = 1360 times greater than that of regular fluorescent cathodes. This means that with this field enhanced thermionic cathode, it is possible to achieve the same electron emission capability at a much lower temperature. It can be estimated that with this field enhanced emission cathode, the operating temperature can be lowered about 300 ^oC without reducing the electron emission capability. It can be also estimated that the cathode temperature change in a typical dimming operation is less then 300 ^oC. Thus, it is feasible to dim a fluorescent lamp without auxiliary cathode heating using this low temperature field enhanced thermionic cathode. And same is true for load shedding operation.

Since this low temperature thermionic cathode can maintain the level of electron emission needed for lamp operation at a much lower temperature, it does not need to be heated up when lamp current is reduced. In the other words, this cathode can operate in a dimming mode without additional cathode heating. Elimination of the need for cathode heating automatically eliminates the possibility of improper auxiliary cathode heating which has been the cause for poor lamp life performance.

Detailed research and development efforts for a prototype low temperature cathode were documented in the following sections.

B. CNT Growth

CNTs were discovered by Ijima in the soot on graphite electrodes following an electrical discharge process that was intended to produce fullerenes (C_{60}). In this process, an arc discharges between the two graphite electrodes while an inert gas is introduced into the system. The CNTs formed on the negative electrode. The high temperature caused by the discharge causes the carbon to sublimate, forming carbon nanotubes. Pure graphite electrodes, or graphite and metal mixtures may be used, with various results. Another method for producing CNTs is laser ablation. A pulsed laser is used to vaporize a graphite target in a high temperature furnace with an inert gas flowing. The cooler surfaces of the growth chamber develop a soot containing CNTs. A water-cooled surface can be included in the system to help in the collection of CNTs. Neither of these processes are able to produce CNTs on a substrate for the purposes of applications; rather, they must be collected from their growth sites. The arc discharge method can be used to produce gram quantities of CNTs, but they are usually mixed in with a large amount of amorphous carbon. Laser ablation can be used to produce CNTs with greater purity, but the quantities are smaller.

Chemical vapor deposition (CVD) has become a widely used method of producing CNTs. The catalytic formation of carbon filaments from the decomposition of carbon gases over metal surfaces was first observed in 1959. However, it was not until 1993 that it was discovered that vapor phase deposition of carbon was capable of producing carbon nanotubes. In this study, a graphite sample was impregnated with iron in a 2.5 % by weight composition. CNTs were formed by flowing acetylene (C_2H_2) and N_2 gases at atmospheric pressure while heating the sample to 700 °C. The deposition process took several hours. It was later recognized that the metal particles became the sites of the CNTs. L. C. Qin *et al.* proposed a model for the CNT growth mechanism in CVD. In this model, the decomposition of the carbon-containing gas took place at the surface of the catalyst particles, leading to carbon deposition on the surface. The heat loss due to chemical changes at the surface and the continued heating of the catalyst lead to a temperature gradient that allows the nanotubes to grow from the catalyst surface while the catalyst itself stays on the substrate surface. However, in many cases the catalyst particles have been observed to stay at the CNT tips as the tubes grow. Both tip growth and base growth have been observed, and can be explained by the strength of the adhesion between the catalyst and the substrate. This was confirmed by K. Song *et al.*, who studied the growth of CNTs on various substrates.

Of all the various methods to produce CNTs, CVD is perhaps the most important for applications, for various reasons. A key advantage is that is possible to grow CNTs directly on the intended substrate by depositing particles of catalyst on the substrate. A common practice for forming particles of catalyst is to deposit a thin film of the metal on the substrate. The thin film of metal can then be etched in plasma, or annealed. Controlled deposition of catalyst leads to the production of CNTs on well defined areas. Another advantage of CVD is that it is possible to grow CNTs on a large or irregular area. CVD is the most promising production mechanism for industrial production. Finally, one of the most important advantages of CVD is that, by generating a plasma in the gas during the CNT deposition, it is possible to produce vertically aligned CNTs. This is called plasma-enhanced CVD (PECVD). This is the growth mechanism used in the current work.

The growth of vertically aligned CNTs was first reported by W. Li *et al*. The catalyst was prepared by chemical methods, producing a network of porous silica with iron particles contained in the pores. CNTs were deposited by CVD, with iron serving as the catalyst. The direction in which each CNT grew was determined by the direction of each pore, with inclined pores producing tilting CNTs. Another report showed the growth of aligned CNTs in laser-etched tracks. The first report of aligned CNTs grown by a PECVD method was given by Z. F. Ren *et al*. In this case, glass was coated with a thin film of nickel, which was then etched in a DC ammonia (NH_3) plasma to produce Ni nanoparticles. C_2H_2 was introduced into the system to begin growing the CNTs, while the NH_3 flow rate was maintained. A growth time of 10

minutes resulted in the production of CNTs 20 μm in length. The catalyst particles were found at the CNT tips in this experiment. Additionally, the CNTs did not grow without NH_3; for example, if N_2 gas was used instead, no CNTs were formed.

The CNT growth method used in this project is similar to the method described by Z. F. Ren. Fig. 2 shows the PECVD chamber used in the present work for the synthesis of CNTs. This chamber had formerly been used for metal evaporation. The chamber itself consists of a bell jar that sits on a stainless steel plate. The vacuum feedthroughs in this plate consist of a series of holes that have been drilled through, necessitating the production of numerous custom fittings for electrical and gas feedthroughs. The center of the plate connects to a gate valve, on the other side of which there is a mechanical pump and a diffusion pump. The diffusion pump is capable of bringing the pressure down to about 10^{-7} Torr, which is a sufficient base vacuum to begin the CNT deposition process.

The samples are placed on a plate of molybdenum that sits on top of a heater. The heater is powered using the existing power supply that had formerly been used for evaporation, and the heater power is controlled using a variable AC transformer. The temperature of the heater is measured using a thermocouple that is designed to fit inside the base of the heater. Because of the molybdenum plate, there is some discrepancy between the temperature measured by the thermocouple and the actual growth temperature of the CNTs. It is possible to use the color of the plate to visually determine the temperature. Once the plate glows a dull red, the growth temperature has essentially been achieved. The temperature is proportional to the heater power, so it is usually possible to achieve the proper conditions by adjusting the power. However, as the heater ages, it requires more power to produce the same temperature.

During the growth process, gases are bled into the system through a stainless steel tube connecting to a series of mass flow controllers. The MFCs are both valves and flow meters calibrated for a particular gas. The flow rate is measured in standard cubic centimeters per minute (sccm), which is the mass in a quantity of the gas present in a cubic centimeter at standard temperature and pressure. MFCs calibrated for NH_3 and C_2H_2 are used in the system. An MFC for argon has also been included, in order to flow argon into the system during the deposition.

The plasma is generated in the system by the DC biasing of the molybdenum plate. This plate is electrically isolated from the rest of the chamber by a ceramic housing that contains the heater. The process gases are brought into the system by means of a stainless steel tube that is situated directly above the growth area. The termination of this tube acts as the grounding for the plasma, so the direction of the electric field in the plasma is from the molybdenum plate to the gas feedthrough, which on a microscopic scale in the growth area would be perpendicular to the surface of the molybdenum plate, and therefore the samples resting on its surface.

The process is illustrated in Fig. 3. Two kinds of substrates have been used in this work: W coils and W ribbons. The ribbons have been favored during the research because it is easier to calculate the emission area, and they have also proven to be more robust than the coils. The substrate is first cleaned by a three-stage process. First, the substrate is placed in an ultrasound bath in distilled water; second, it is washed in a solution of distilled water, ammonium hydroxide, and hydrogen peroxide, to remove organic contaminants; and finally it is washed in a solution of distilled water, hydrochloric acid, and sulfuric acid to remove oxides. A thin film of Ni is produced on the surface of the substrate by sputter deposition, which is described in the next section.

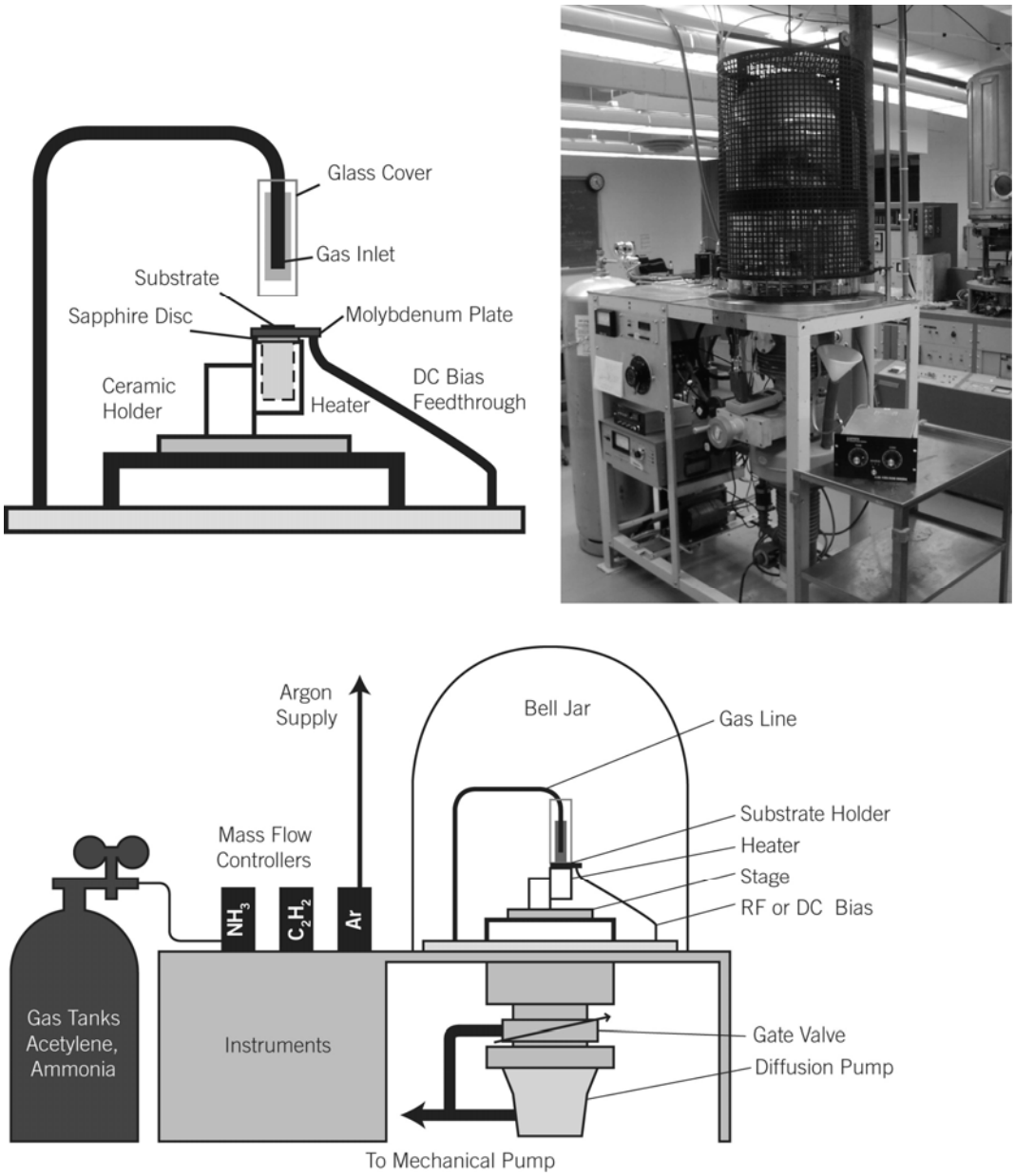

Fig. 2. A diagram of the PECVD chamber used in this system, with a close up of the substrate holder (upper left), and a photograph (upper right).

The Ni may be limited to a small area of the cathode with the use of a mask during the sputter deposition process, in order to have a well-defined emissive area.

The substrate is placed on the molybdenum plate in the PECVD chamber. The chamber is sealed and the pressure is brought down to 10^{-7} Torr. NH_3 and argon are bled into the system by activating the MFCs. 160 sccm of NH_3 and 20 sccm of argon are used. The gate valve is tightened until it is almost closed to regulate the pressure. When the pressure has reached 7–9 Torr, it is possible to attempt to ignite the plasma by turning on the DC bias power. A biasing power of 30 W is generally used, although the amount of power delivered to the system is usually much less than this. If the pressure is too low, no plasma will be generated; on the other hand, if the pressure is too high, the plasma will

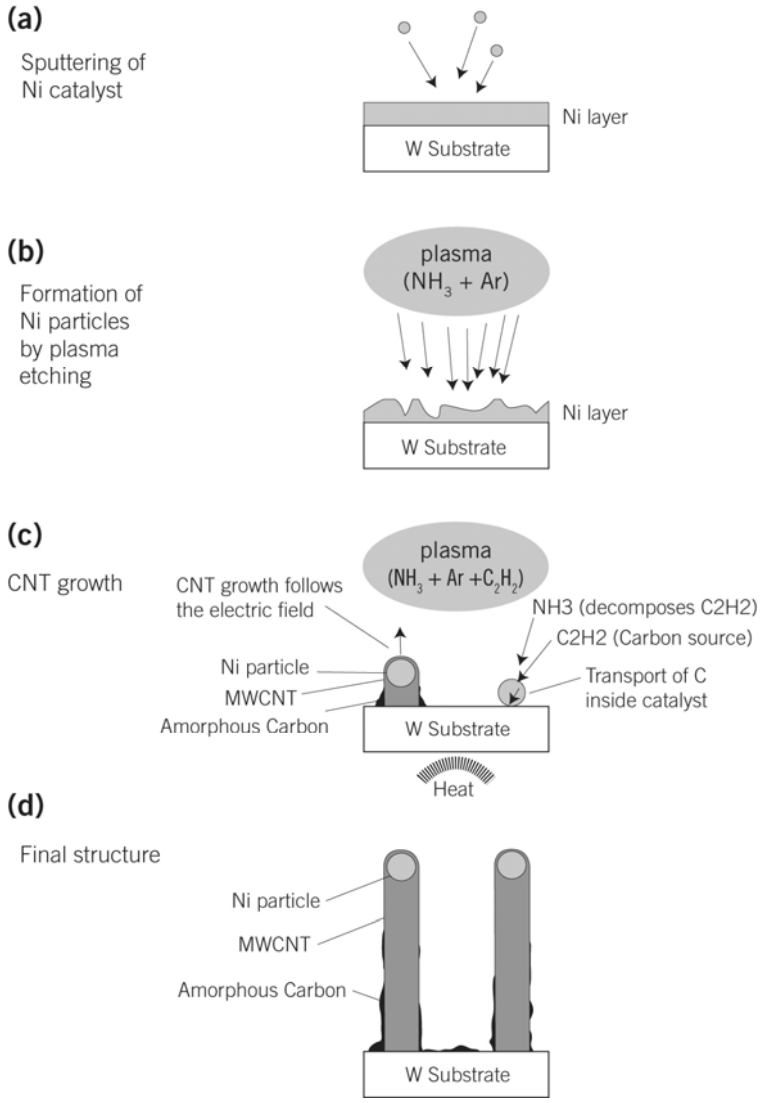

Fig 3. The CNT growth process, with (a) the deposition of Ni by sputtering, (b) NH_3/Ar plasma etching to form Ni nanoparticles, (c) catalytic CNT growth, and (d) the resulting nanostructure.

not be contained to the growth area. Thus, maintaining the pressure at 7–9 Torr is important. The Ni is etched in plasma for 1–10 minutes, varying according to the desired CNT density. At this time, the heater power is slowly brought up to bring the substrate to the growth temperature. The growth temperature is in the range of 600–700 °C as measured by the thermocouple. The heater power is increased slowly to avoid damage. The heat is not required for the plasma breaking of the catalyst, so it may be turned on at any time prior to the CNT growth. The CNT growth process is immediately started with the flow of C_2H_2 into the system by turning on the appropriate MFC. The gas ratio of C_2H_2:NH_3 that has been used for the CNT growth was 80:160 sccm, along with 20 sccm of Ar. The growth time may vary from 15 to 50 minutes or longer, according to the desired CNT length. To stop the CNT growth process, the DC power is turned off. The gate valve is opened and the MFCs are deactivated. The heater power is gradually reduced, and the substrate is allowed to cool.

Using the PECVD system described above, we have mastered the technique for growing CNTs and we were able to grow vertically aligned CNTs on both flat and coil substrates. Figures 4-6 give some examples of the CNTs that we have grown on different types of substrates for our studies.

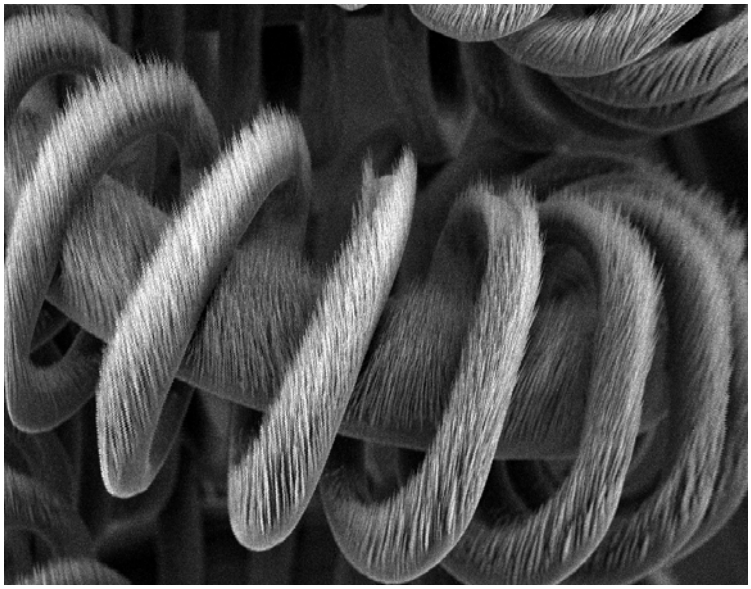

Figure 4. SEM image of CNT grown on tungsten coil.

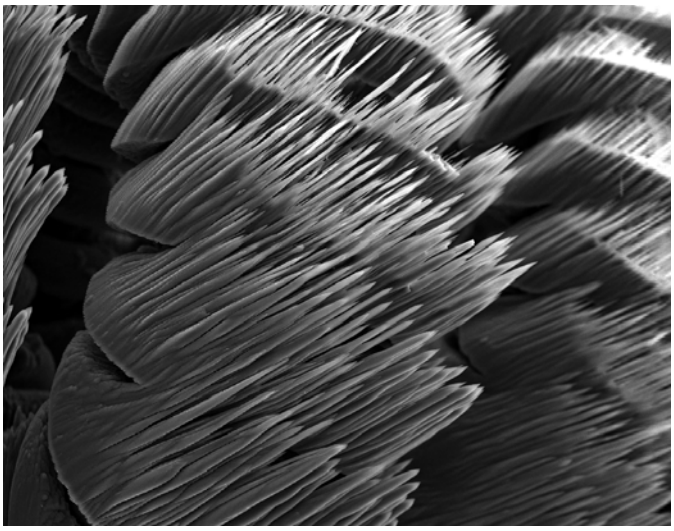

Figure 5. Magnified SEM image of the same sample.

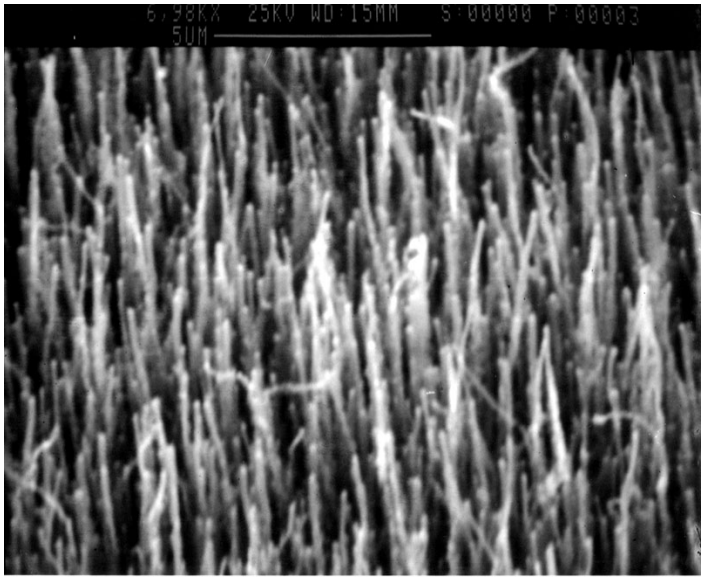

Figure 6. SEM image of CNT grown on flat tungsten ribbon.

The morphology of the CNT template is very important to the oxide coated CNT cathode, as it provides the field effect and enhances electron emission. The field enhancement factor of a field emission cathode consisting of CNTs can be approximated by the expression:

$$\beta = \beta_0\left[1 - \exp(-2.3172 s / l)\right], \qquad (2)$$
$$\beta_0 = 1.2(l / r + 2.15)^{0.9}$$

where s is the average spacing between CNTs, β_0 represents an intrinsic field enhancement factor (i.e., of an average CNT in the emitter), l is the average CNT

length and *r* is the average CNT radius. This expression shows the relationship between emitter spacing, CNT length, and CNT radius. Densely packing emitters close together decreased rather than increased the current density, because of a screening effect. The smaller the spacing between the emitters, the more the electric field behaves as though it were meeting a flat surface. However, the inverse is not necessarily true; rather, there is a maximum value for the field enhancement with respect to the emitter spacing, beyond which there is no additional benefit from spacing out the emitters further. The screening effect is illustrated in Fig. 7. To complicate the issue further, the field enhancement factor is not the only factor that determines the emission, the number of sites that emit, or in the case of thermionic emission; the area of emitting surface, also plays an important role in determining total emission current. One of the major efforts in this research will be to examine the impact of the surface morphology of CNTs on thermionic emission of the oxide coated CNT cathode.

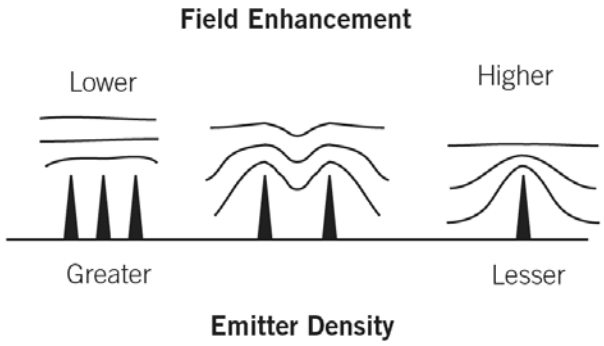

Fig. 7. Illustration of the screening effect in arrays of field emitters.

While the length of the CNTs can be controlled simply by adjusting the growth time, the density and the spacing of the CNTs can be controlled by the thickness of the Ni catalyst thin film and the etching time as shown in the following example. Starting with a thin film of Ni with a thickness of 100 nm, different morphologies were established by varying the etching time. Etching for 1 min produced a very dense film of CNTs with a density of approximately 3×10^8 cm^{-2}. Using a 5-min etching time reduced the density to about $0.5–1 \times 10^8$ cm^{-2}, while etching for 10 min reduced the density to about 5×10^7 cm^{-2}. Using 60-min growth time produced CNTs with lengths of about 15 μm, while 30-min growth time produced CNTs with lengths of 8 μm. The length of the CNTs was dependent mostly on the growth time, while the density was dependent on the etching time. SEM images of these samples are shown in Fig. 8. A direct comparison of thin films of Ni catalyst particles with different densities, and the CNTs grown from them, is given by the SEM images in Fig. 9.

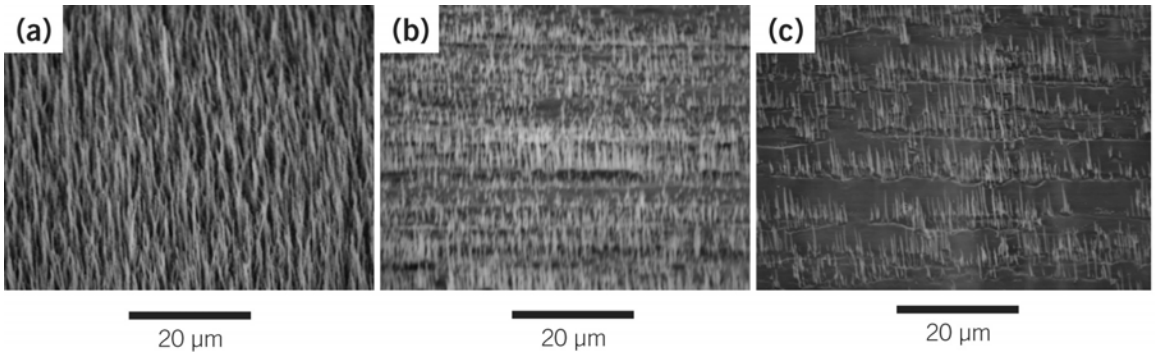

Fig. 8. SEM images of CNT samples grown using 100 nm Ni, with (a) 1 min etching time and 60 min growth time; (b) 5 min etching time and 30 min growth time; (c) 10 min etching time and 30 min growth time. The SEM tilt angle is 45° in all images.

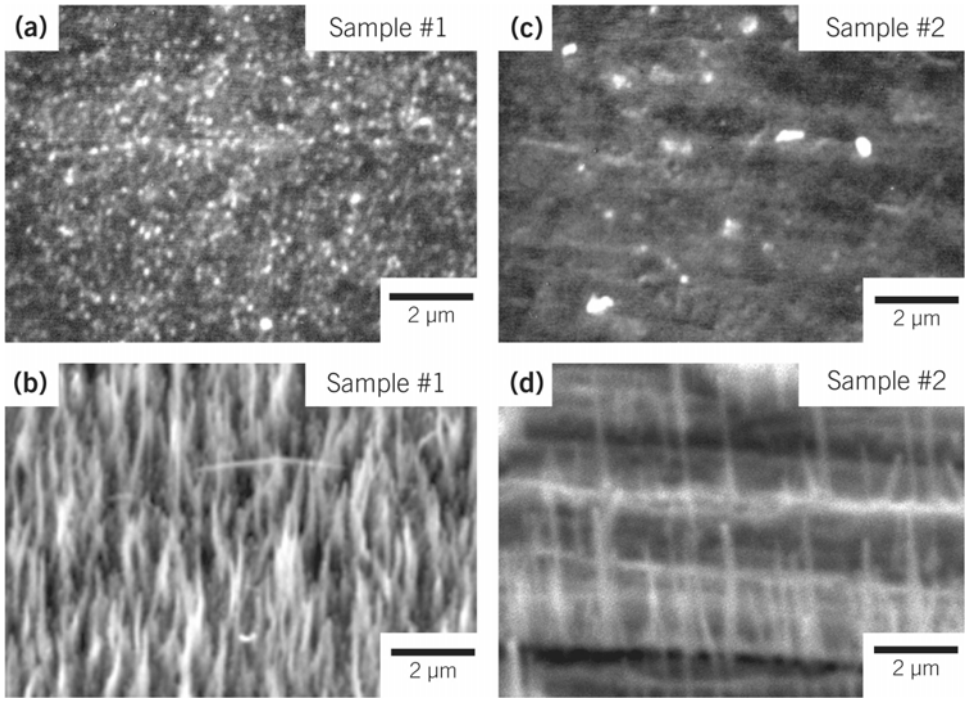

Fig. 9. SEM images of Ni catalyst particles and the corresponding CNT films. Sample #1 (a, b) and Sample #2 (c, d) correspond to Fig. 3 (a) and (c). The SEM tilt angle is 45° in all images.

With the ability to control the morphology of the CNTs samples, we have conducted a numerous detailed studies on the correlation between CNT morphology and the field emission and field enhancement factor. The following example studied the effect of length and spacing of CNTs on field emission and field enhancement factor. Figure 10 are some of the examples of the CNT that we studied. These samples have different tube lengths and spacing. Their emission characteristics are

shown in figure 11. Finally the emission characteristics of these carbon nanotubes samples are also summarized in table 1.
The morphology of the carbon nanotubes thin film (mostly tube length, spacing and alignment) determines the field enhancement factor of the carbon nanotubes samples, which in turn affect the field enhancement factor of the cathode. Therefore, the knowledge of the relationship between the field enhancement factor and the CNT morphology, and the ability to control the morphology of the CNT samples are important to optimize the overall performance of the field enhanced thermionic cathodes.

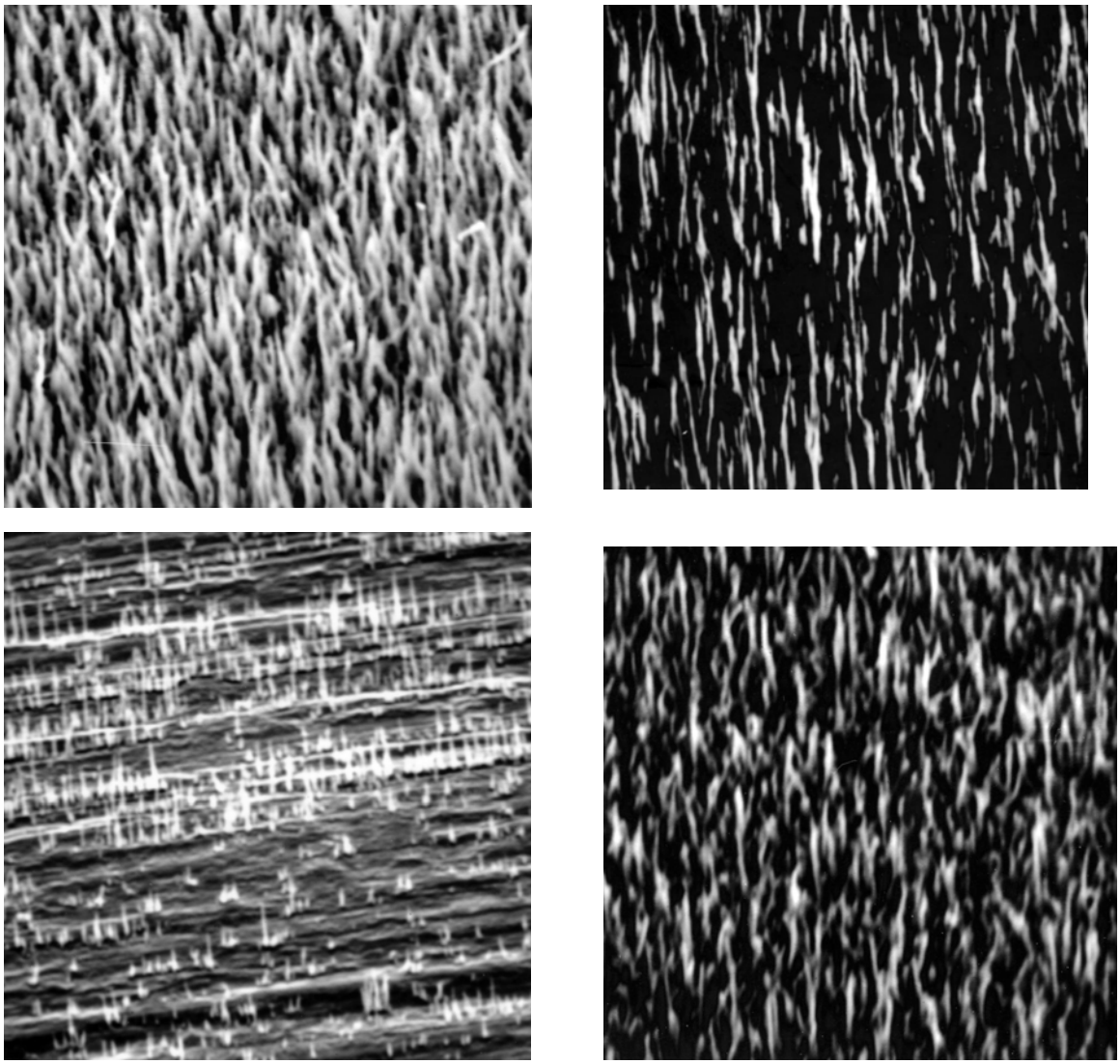

Figure 10: SEM image of various CNT grown on tungsten Foils.

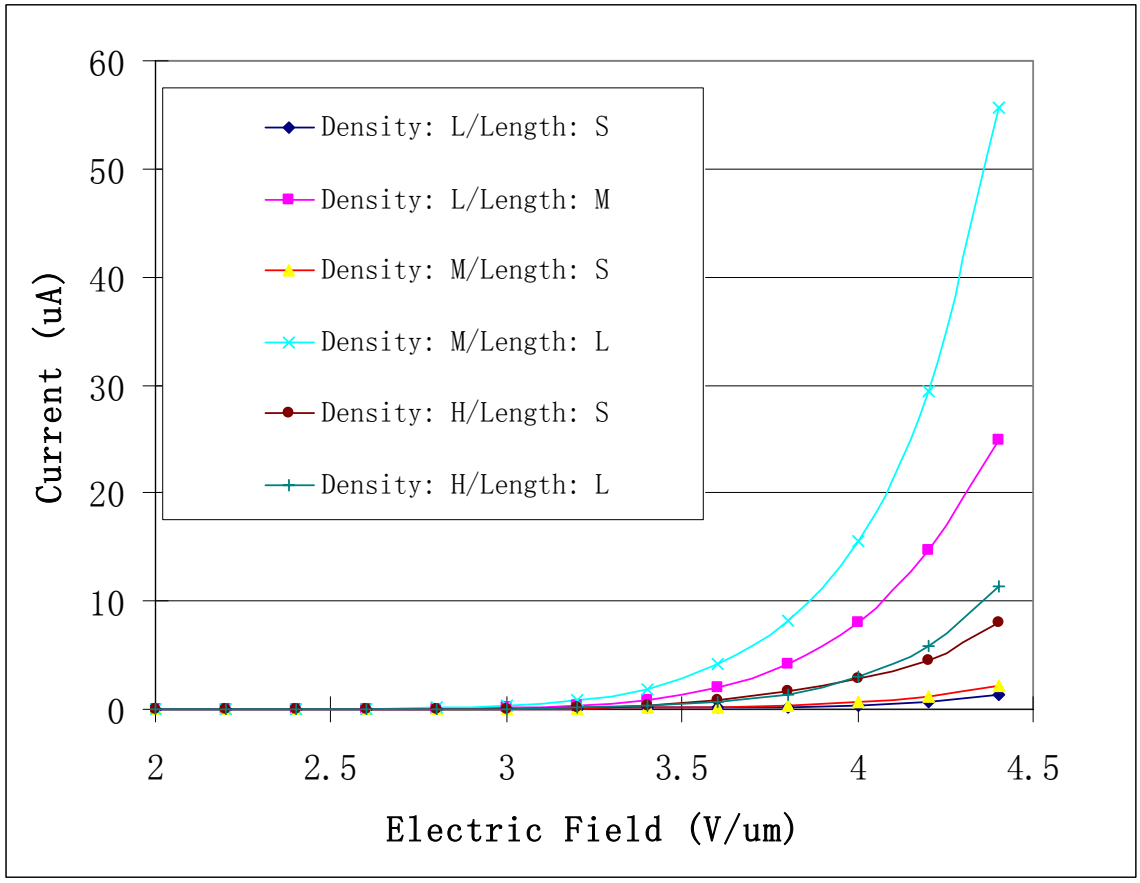

Figure 11. I-V curves for CNT samples with various morphologies

Table 1. Summary of Emission Properties of Various CNT Samples

CNTs	Density (Spacing)	Length	I (uA) at 4.4V/um	F-N slope	Field Enhancement Factor Beta
0328 100nm_10rt-15	Low	Short	1.3	-583773	1099
0206 50nm_5-50	Low	Medium	24.9	-422097	1520
0404 100nm_7.5rt-15	Medium	Short	2.1	-427536	1500
0428 100nm_5rt-60	Medium	Long	55.7	-418805	1532
0327 100nm_5rt-15	High	Short	8	-374675	1712
0323 100nm 1-60	High	Long	11.4	-432149	1484

C. Oxide Deposition and Prototype Cathode Development

Magnetron sputtering technique was used to deposit thin film of oxide onto CNT surface in this project. Sputtering is a relatively simple thin film deposition process that is commonly used because of its many advantageous properties. Sputtering produces thin films with excellent uniformity and adhesion, at high rates of deposition that are easily controlled. Most materials can be deposited by this method because the deposition process depends on momentum exchange, and there is no chemical reaction involved. Metals, especially elemental metals, are particularly easy to deposit by sputtering. Compounds can be deposited either by the sputtering of those compounds in solid state, or by reactive sputtering of an element in the compound with a reactive gas (such as an oxide by sputtering of a metal and O_2). Another advantage of sputtering is that it can be scaled from a laboratory to a manufacturing setting. For these reasons, sputtering was chosen as the method for deposition of thin films in this experiment.

Depending on whether the source materials are dielectric or metallic, magnetron or non-magnetron sputtering may be used. In non-magnetron sputtering, a metal target, usually a disk, is mounted on the sputtering source, which provides the voltage to ignite the plasma. Because the target acts as a cathode in generating the plasma, this arrangement is called diode sputtering. If a heated filament is also added to the sputter source, this is called triode sputtering. The purpose of the filament is to improve the plasma, enabling operation at lower pressures and lower voltages.

Dielectric materials must be deposited using magnetron sputtering, because they cannot be a cathode for the generation of a plasma. Instead, the plasma is generated by a strong magnetic field produced by an magnet, usually in a circular configuration with the north end of in the center and the south end at the edges. This is illustrated in Fig. 12 (a). In combination with the electric field, the effect is to confine electrons to a region near to the target surface, which influences the flow of ions, improving the sputtering rate. Magnetron sputtering allows lower pressures and voltages to be used. Both DC and RF power can be used for magnetron sputtering, although RF is required for sputtering dielectric materials. One disadvantage of magnetron sputtering is that the erosion of the target is uneven, being greatest where the magnetic field lines are parallel to the target surface. This is illustrated in Fig. 12(c) and (d).

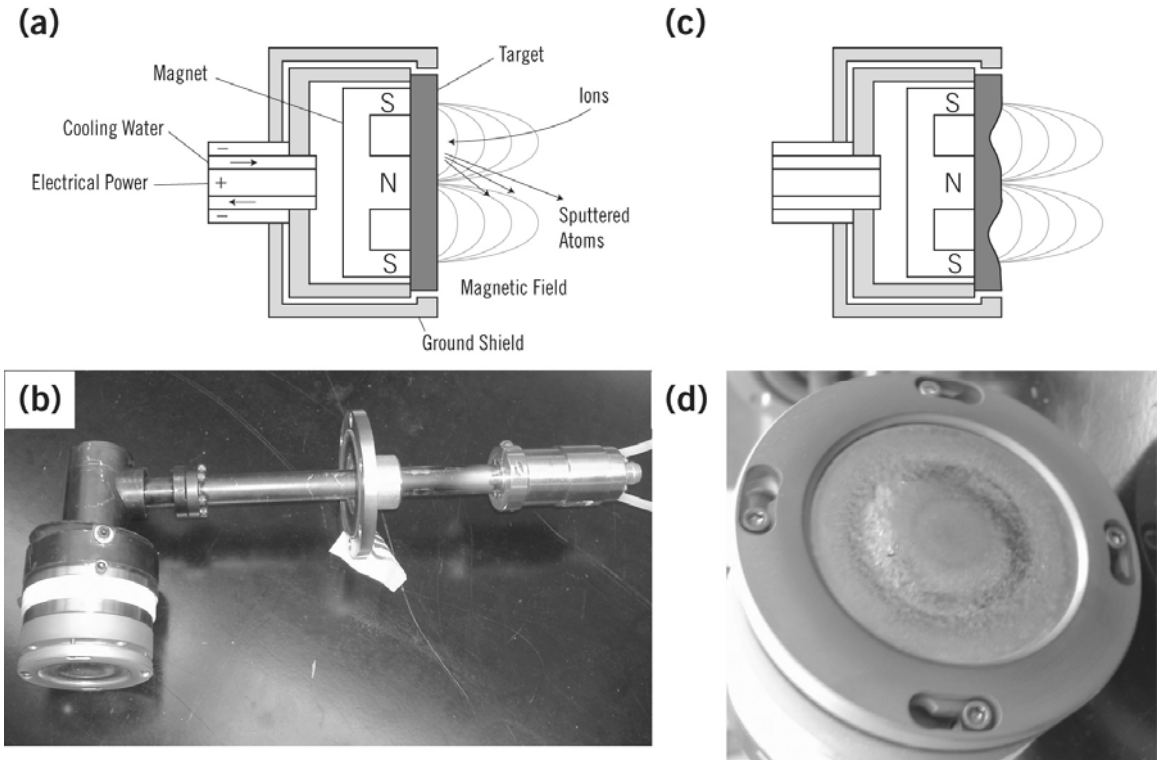

Fig. 12. (a) The cross section of a magnetron sputtering source; (b) a picture of a sputter gun; (c) the cross section of a target after long use; and (d) a close-up picture of a used sputtering target showing the uneven erosion of materials.

The particles sputtered from the source material are usually single atoms. For example, if an alloy is used, the substrate is often coated preferentially with one of the alloy's elemental components. For dielectric compounds such as oxides or nitrides, it is possible to sputter a solid target of the actual material using RF power. However, forming solid targets of this kind of material is usually difficult, and such targets experience cracking due to poor thermal conductivity. Reactive sputtering is a more effective method for creating dielectric films. In this process, the target is composed of the metallic element in the desired thin film, while the other element in the desired film is leaked into the chamber. For example, aluminum nitride (AlN) could be produced by sputtering an Al target while flowing N_2 into the system. Likewise, Al_2O_3 could be produced by flowing O_2 rather than N_2, which illustrates the versatility of reactive sputtering. The reactive gas may be introduced near to the substrate or near to the target materials. For oxides, the former configuration is often used, while for nitrides, the latter.

The sputtering chamber used in this work consists of a vacuum collar situated on a stainless steel plate, onto which a stainless steel dome is lowered. The weight of the dome is sufficient to create a seal between its bottom surface and the collar, and the weight of the collar and the components installed in its walls are sufficient to create a seal between the base of the collar and the bottom plate. Viton rubber O-rings make the seals between these components. The dome is raised and lowered by a

mechanical lift installed on a gantry above the system. A gate valve connected this chamber to a mechanical pump and a turbo pump. The minimum pressure observed in this chamber has been a low 10^7 Torr. The turbo pump is capable of producing much lower pressure, but the large size of the chamber and the use of large O-ring seals limits the vacuum. The pressure in this chamber is measured using a capacitance manometer.

Five magnetron sputtering guns were used in this system. They were mounted on the dome. Four RF power supplies were available for use in this system, including two Dressler Cesars, an Advanced Energy RFX-600 and a Seren AJA 100/300. These all had automatic matching networks except the Seren, which had a manual matching network. One DC power supply was available, an Advanced Energy MDX-500. The sputtering guns were cooled by water that was delivered by a network of plastic tubing. The three automatic matching networks were mounted on the dome of the sputtering system to make the distance between the output of these matching networks and the input of the sputtering guns as short as possible, in order to minimize the RF power loss. Each sputtering gun had a target of source material mounted on the vacuum side, and up to five different materials could be sputtered at the same time with this system. Each sputtering gun had a shutter that can be used to control the deposition without changing the power off.

The substrate holder is located in the center of the bottom plate. Because it is level, no additional support is needed for the substrate. The holder sits on a rotating shaft whose speed is controlled by an external unit. Two heaters are in place beneath the holder, and their temperature is controlled by an external unit that measures the temperature using a thermocouple, and can automatically turn on and off the heaters to maintain a constant temperature. The substrate holder may be biased with an external power source. Finally, a shutter is installed to cover the substrate before the deposition. This is helpful for better controlling the deposition time. In this work, targets of alkaline metal were used, which reacted strongly with air when the chamber was opened for the removal of substrates. It was necessary to clean the surfaces of these substrates by sputtering before the deposition. The shutter prevented deposition of unwanted materials on the substrate.

There are two gas inlets for the sputtering system. The inert gas is leaked into the chamber with one, while the other directs the reactive gas near to the substrate with the use of a stainless steel tube bent into a circular shape, with vents pointing toward the substrate. A crystal thickness monitor is used to measure the deposition rate and the total amount of deposition. Argon was used for the inert gas in this experiment. Gas flow rates were controlled using MFCs as in the PECVD chamber.

For the present work, this chamber has been used to deposit films of Ni, W, BaO and SrO. This system was used to deposit thin films of Ni for use as catalyst in the growth of CNTs. Reactive sputtering with pure Ba and Sr targets and O_2 was used

to produce the oxides. W ribbons and CNTs were both coated successfully with BaO/SrO and Ni, with little change in the CNT morphology, as shown in Figs. 13 and 14. Fig. 13 contains SEM images of oxide films produced with this system. The surface of a thick oxide layer is shown in Fig. 13(a). Oxide coated CNTs are shown in 13(b), compared with uncoated CNTs in 13 (c) to demonstrate that the CNT alignment remains undamaged. Fig. 14 shows TEM images of CNTs produced with this system. Also, a diagram of the sputtering system is shown in Fig. 15.

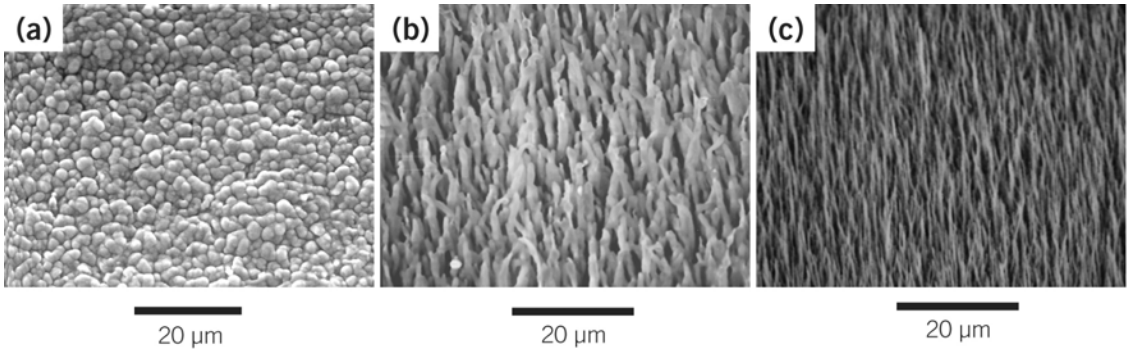

Fig. 13. SEM images of thin films of BaO/SrO coated by reactive magnetron sputtering onto (a) the flat surface of a W ribbon, and (b) a W ribbon with CNTs. For comparison, an SEM image of uncoated CNTs (c) is also shown. An SEM tilt angle of 45° was used for all images.

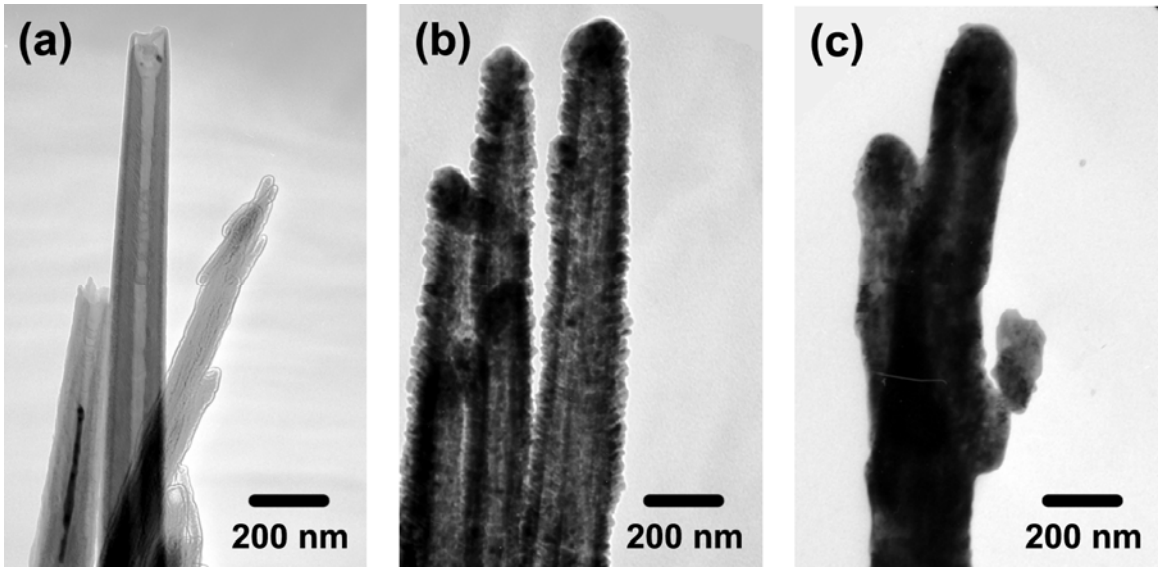

Fig. 14. TEM images of (a) an uncoated CNT, (b) a CNT coated with Ni, and (c) a nanotube coated with BaO/SrO.

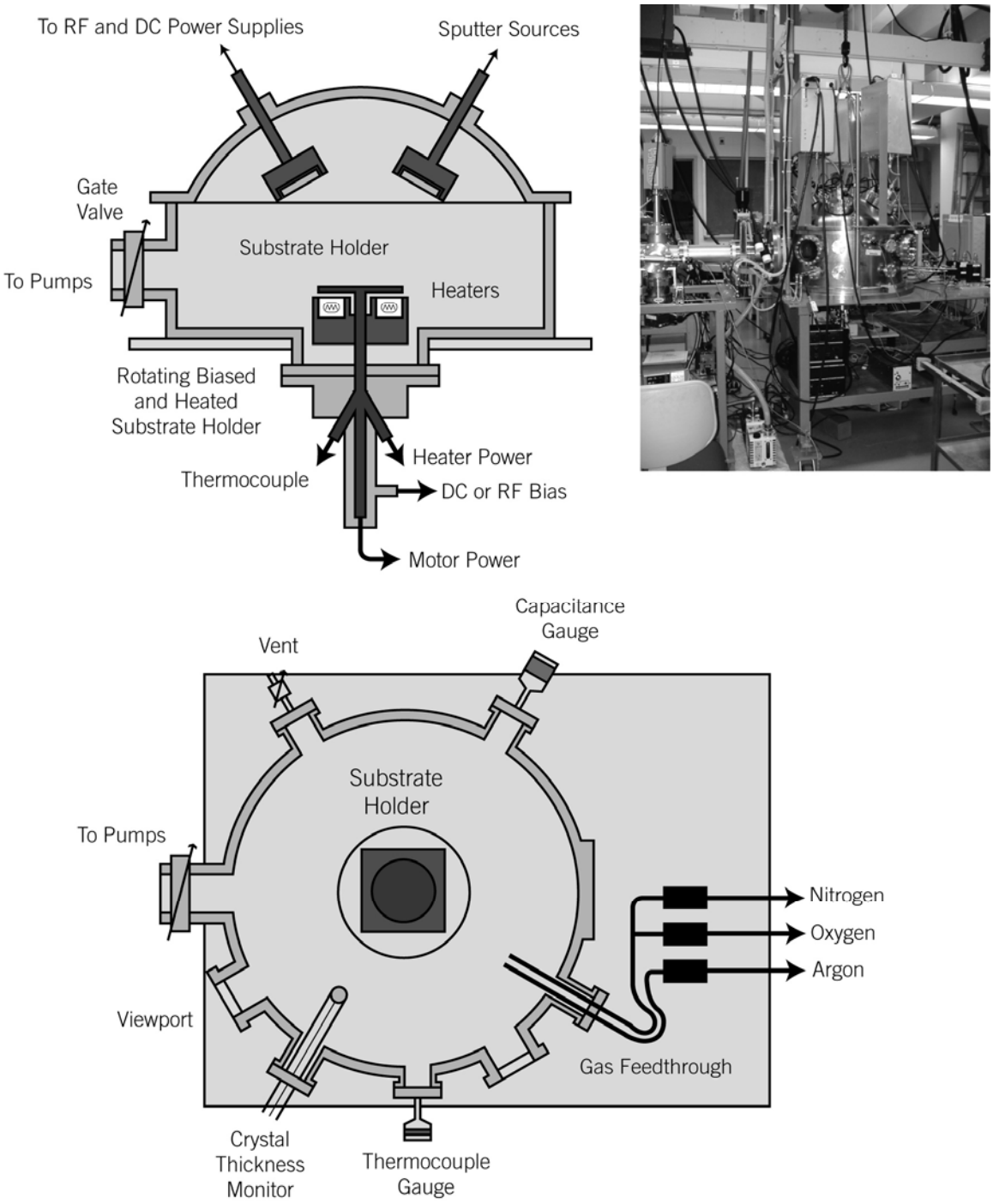

Fig. 15. A diagram of the sputtering system, showing side view (upper left) and top view (bottom) cross sections, along with a photograph (upper right).

The cathode structure proposed in this study consists of oxide coated carbon nanotubes deposited on a W ribbon. The size of oxide particles as the kind that are deposited by conventional means (the painting or spraying of a carbonate powder) are very large compared to the size of the nanotubes. Dumping a large amount of this material on the CNTs would obscure the nanotube geometry as well as mask the field enhancement that the nanotubes might have provided. For this reason, thin film oxide

is desired as coating materials in this project. By using a thin film of oxide, it was possible to retain the overall nanotube geometry, thereby preserving the field enhancement factor (with some loss due to the increase of the nanotube radii). The oxide coating would lower the work function of the emitting surface, thereby increasing the emission dramatically compared to the uncoated nanotubes.

Previously, the thin film deposition of oxides for cathodes has not been considered. This research is the first to report the successful deposition of BaO/SrO by reactive sputtering for the purpose of creating an electron emitter. A number of adjustable growth conditions were controllable during the deposition. A series of emission measurements were carried out on oxide coated tungsten samples to determine the effects various growth parameters on the quality and emission properties of the oxides. In this section, the results of one study are presented. The parameters chosen for the oxide deposition in this study were decided on after a large number of preliminary tests.

In the following examples, (BaSr)O thin films were deposited in the magnetron sputtering deposition system with a base pressure below 5×10^{-7} Torr. Tungsten ribbons ($30 \times 0.038 \times 0.76$ mm) treated with the RCA cleaning process were used as substrates on which the oxide films were deposited. The size of the oxide film was limited to an area of 0.012 cm^2 by masking the tungsten ribbons. Two 3-inch diameter targets of pure barium and strontium (> 99.5% purity) were mounted on two independent sputtering guns and co-sputtered in argon and oxygen gases at a pressure of 1 mTorr. The ratio of oxygen to argon gas flow was 1:10 and was maintained at a total rate of 11 sccm (standard cubic centimeters per minute at STP). Three cathodes were prepared at different substrate temperatures: 25 °C, 400 °C and 700 °C. The substrate was rotated at 30 rpm to ensure the uniformity of the film thickness. The RF power applied to the Ba and Sr targets were 150 W and 100 W respectively, leading to a deposition rate of 3.0 Å/s. The sputtering rate and thickness of the oxide film was monitored by a thin film thickness monitor during the deposition. All the oxide films reported in this work have a thickness of approximately 1 μm.

Fig. 16 shows the top-view SEM micrographs of as-deposited (BaSr)O films sputtered on tungsten substrates at different substrate temperatures of (a) 25 °C, (c) 400 °C, and (d) 700 °C. Overall, the oxide films were polycrystalline and appeared continuous, covering the entire surface of the tungsten substrates. The effect of substrate temperature on the surface morphology and structure of the oxide films are revealed by the SEM images. The (BaSr)O film deposited at 25 °C [Fig. 16(a)] had a rough surface with a macroscopic quasi-grain structure. The sizes of the quasi-grains were large and non-uniform, with diameters of approximately 11 μm. These large quasi-grains contained a sub-structure of nanocrystalline sub-grains with an average size of about 300 nm, which can be seen in the high magnification SEM image in Fig. 16(b). These kinds of structural features are typical for sputtered thin films deposited

at low substrate temperatures, due to the low surface mobility of adatoms. With increased temperature, the oxide films started to show a smoother surface and an improved polycrystalline structure. At a substrate temperature of 400 °C, the (BaSr)O film shown in Fig. 16(c) had more uniform grains separated by clear grain boundaries, and the grain sizes were about 2 μm. The (BaSr)O film deposited at 700 °C [Fig. 16(d)] had the smoothest and flattest surface with the most closely packed grain structure. The identifiable grains were approximately 3 μm in size. The change of the oxide film structure due to substrate temperature can be explained as follows: at high substrate temperatures, high surface mobility of adatoms encouraged the nucleation, growth, and merging of the grains, forming a smooth film with higher mass density and grain size. The RF powers applied to the Ba and Sr targets were fixed at 150 W and 100 W respectively. The RF powers determined the sputtering rate, which in turn determined the composition of the oxide films. The energy-dispersive spectrum of an as-deposited (BaSr)O film is presented in Fig. 17. The EDS result shows that the ratio of Ba to Sr in the film is about 1:1 in atomic percentage.

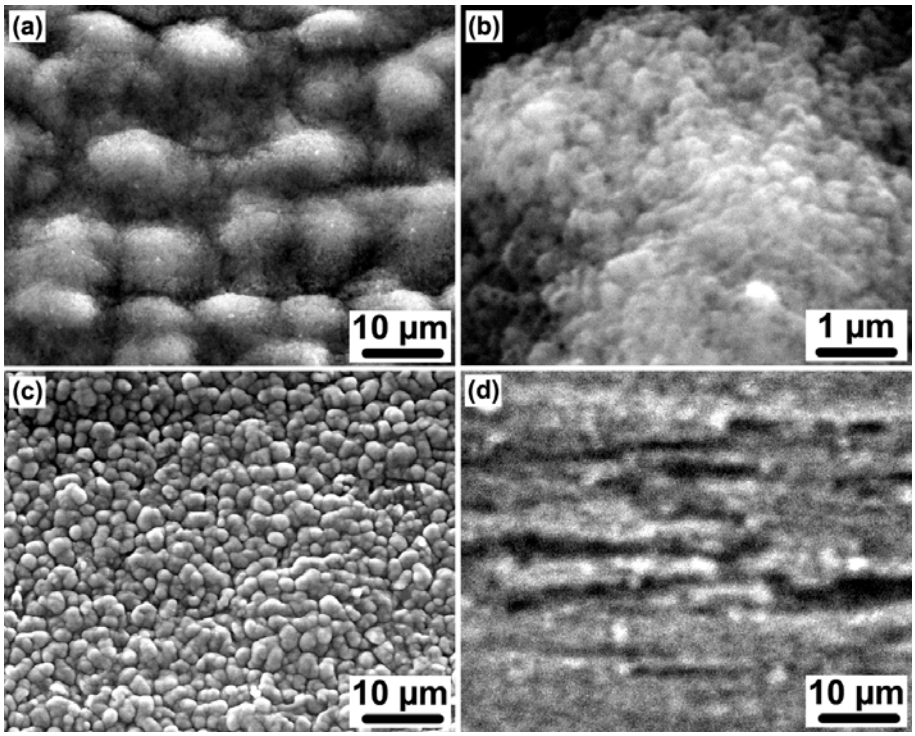

Fig. 16. SEM micrographs of as-deposited (BaSr)O films on tungsten at substrate temperatures of (a) and (b) 25 °C, (c) 400 °C and (d) 700 °C.

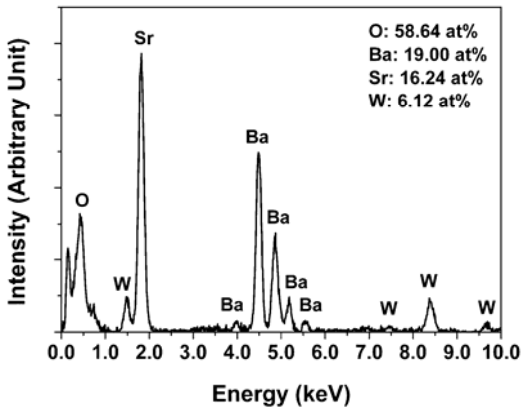

Fig. 17. Chemical composition of an as-deposited (BaSr)O film by EDS analysis.

Fig. 18 shows the thermionic emission current density versus electric field at various temperatures for the (BaSr)O films deposited with substrate temperatures of (a) 25 °C, (b) 400 °C, and (c) 700 °C. These emission current density-electric field (J-E) plots show similar characteristics: an onset emission current at zero field, a rapid increase in emission current, and a linear saturation region of emission current at fields above 0.08 V/μm. Values for the emission current density were calculated using the measured current values and the surface area of 0.012 cm^2. The emission current densities from the oxide films under an electric field of 0.88 V/μm at a series of cathode temperatures are reported in Table 1. Within the temperature range from 1209 K to 1097 K, the (BaSr)O film deposited at 700 °C had the largest emission current density, ranging from 1.60 A/cm^2 to 0.44 A/cm^2, approximately twice that of the (BaSr)O film deposited at 400 °C and three times that of the (BaSr)O film deposited at 25 °C at equivalent temperatures.

Figs. 19(a), (b) and (c) show the corresponding Schottky plots for the (BaSr)O films deposited at substrate temperatures of 25 °C, 400 °C, and 700 °C respectively. Values of the zero field emission at different cathode temperatures were extrapolated from the linear portions of the Schottky plots, and used to generate the Richardson plots shown in Fig 19(d). The Richardson plots for all three oxide films fit straight lines well. The work functions were calculated using the slopes of the fitting lines, and the emission coefficients were calculated using the intercepts. The calculated work function and emission coefficient values are summarized in Table 2. The results are consistent with the measurements of emission current density. The (BaSr)O film deposited at 700 °C had the largest emission current density, and the lowest work function, 1.57 eV. The (BaSr)O films deposited at 400 °C and 25 °C had relatively higher work functions of 1.72 eV and 1.85 eV, respectively.

The chemical compositions of the three sputtered (BaSr)O films were similar. The differences in thermionic emission performance can be explained by structural differences in the films resulting from the use of different substrate temperatures during oxide deposition. High temperature deposition resulted in a smooth surface, a

uniformly close-packed crystalline structure, and possibly a better intermixing of BaO and SrO phases. All of these features can enhance the metal-oxide interaction, Ba transportation, and electron conduction, leading to a low work function and high emission current density. In contrast, low temperature deposition produced a rough surface and uneven crystallinity in the oxide film, resulting in a relatively high work function and low emission current density. Compared to the traditional oxide cathodes, the oxide thin film cathodes made by RF magnetron sputtering should have a greater mass density due to the absence of pores left behind when the carbonates are converted into the oxides during the activation. The smooth surface and nonporous close-packed crystalline structure of the oxide film sputtered at high substrate temperature are presumed to provide better resistance to attacks from the residual gases in a working environment.

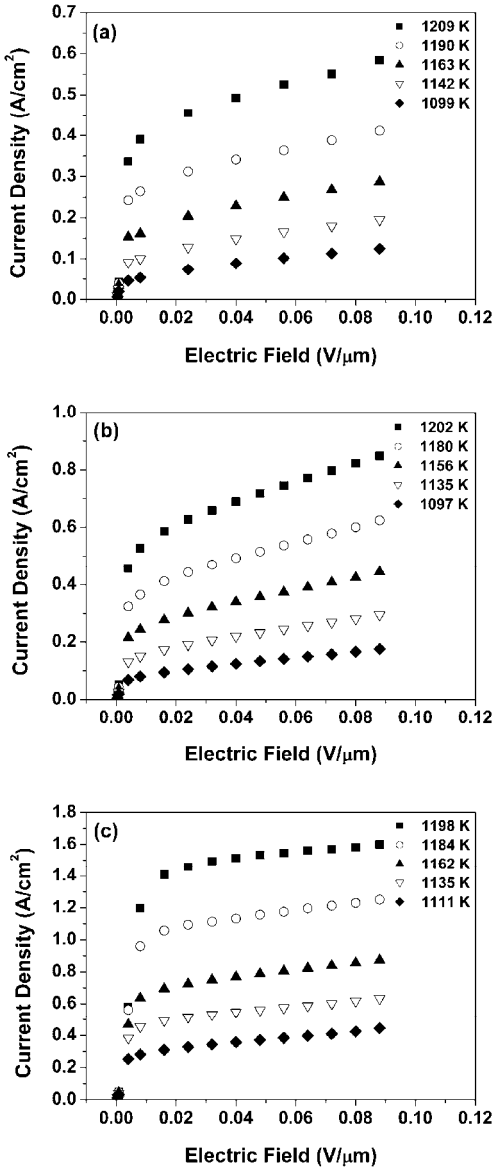

Fig. 18. J-E plots of (BaSr)O films deposited at substrate temperatures of (a) 25 °C, (b) 400 °C, and (c) 700 °C.

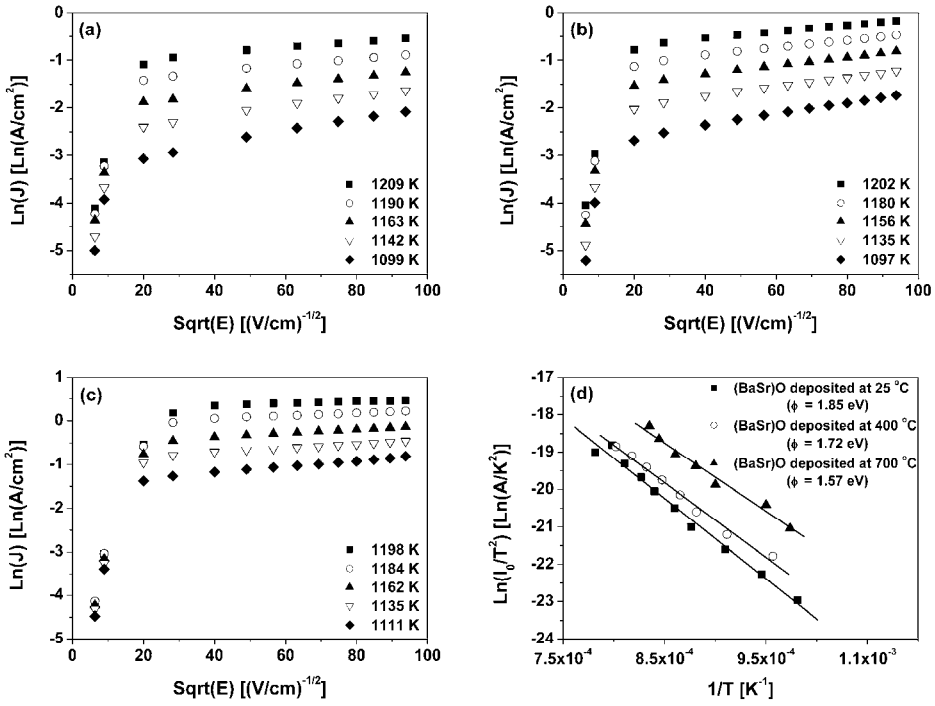

Fig. 19. Schottky plots of (BaSr)O films deposited at substrate temperatures of (a) 25 °C, (b) 400 °C, (c) 700 °C, and (d) the corresponding Richardson plots.

Table 1. Thermionic emission current densities at various cathode temperatures from (BaSr)O films deposited at substrate temperatures of 25 °C, 400 °C, and 700 °C.

Substrate Temperature (°C)						
25	Cathode Temperature (K)	1209	1190	1163	1142	1099
	Emission Current Density (A/cm^2)	0.58	0.41	0.29	0.20	0.12
400	Cathode Temperature (K)	1202	1180	1156	1135	1097
	Emission Current Density (A/cm^2)	0.85	0.62	0.44	0.29	0.18
700	Cathode Temperature (K)	1198	1184	1162	1135	1111
	Emission Current Density (A/cm^2)	1.60	1.25	0.87	0.63	0.44

Table 2. Work functions and emission coefficients of (BaSr)O films deposited at substrate temperatures of 25 °C, 400 °C, and 700 °C.

Substrate Temperature (°C)	Work Function (eV)	Emission Coefficient ($A \cdot cm^{-2}K^{-2}$)
25	1.85	11.56
400	1.72	4.97
700	1.57	3.21

Having acquired the knowledge of depositing thin film oxide on flat surfaces, we started experimenting depositing such oxide thin films onto the CNT surfaces to create the oxide coated CNT cathodes. A large number of experiments were conducted and many samples were created. The following example is used to illustrate the improved emission from the coated CNTs as compared to the uncoated CNTs, and thus the benefit of the low work function surface coating.

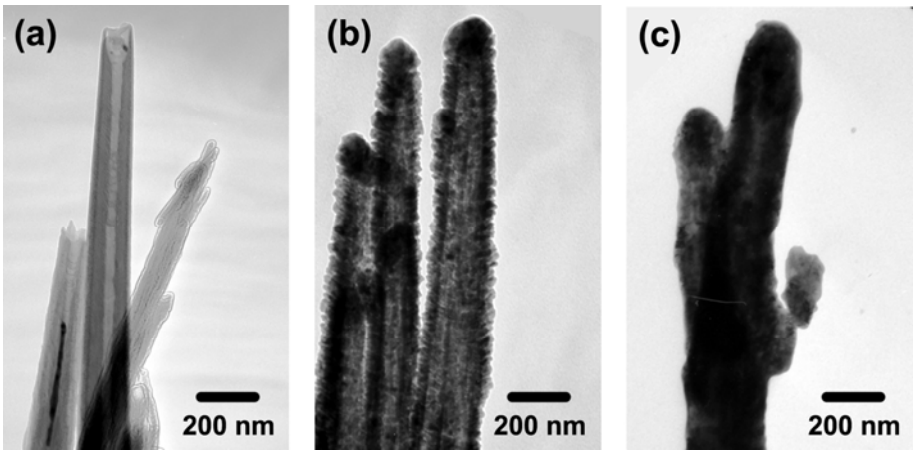

Fig. 20 (same as figure 20). TEM images of uncoated CNTs (a), 50 nm nickel coated CNTs (b), and 100 nm barium strontium oxide coated CNTs (c).

Barium strontium oxide (BaO/SrO) was chosen as the surface coating and they were deposit in the same manner at 700 ^{o}C as described earlier. By properly adjusting the deposition parameters, we were able to use magnetron sputtering to deposit both metal and oxide thin films on the surface of the CNTs. Fig. 20(a), (b) and (c) are TEM images of individual CNTs, nickel coated CNTs and oxide coated CNTs respectively. The metal and oxide surface coatings can be clearly seen from Fig. 20(b) and (c). The thickness of the nickel coating was approximately 50 nm, and the oxide coating was approximately 100 nm thick. Both coatings were fairly uniform and covered the whole

surface of the CNTs. The overall shape of the coated CNTs was similar to that of the uncoated CNTs, while their diameters were increased due to the additional surface coatings. The formation of the oxide and nickel coatings on the CNT surfaces was confirmed with chemical analysis using energy-dispersive spectrometry (EDS). Fig. 21(a), (b) and (c) show the SEM images of the uncoated CNTs, nickel coated CNTs and oxide coated CNTs respectively. The CNT samples used here were from the same batch as sample A in the previous section. The diameters of the oxide coated and nickel coated CNTs appeared thicker than the uncoated ones in the SEM images, while the overall surface morphology and the alignment of the coated CNTs remained largely unchanged by the deposition of the surface coatings. These TEM and SEM images clearly demonstrated the ability of the magnetron sputtering technique to deposit uniform thin films on extremely uneven surfaces like CNTs. This technique can be a versatile tool in functionalizing CNT surfaces with a variety of metal and dielectric functional materials.

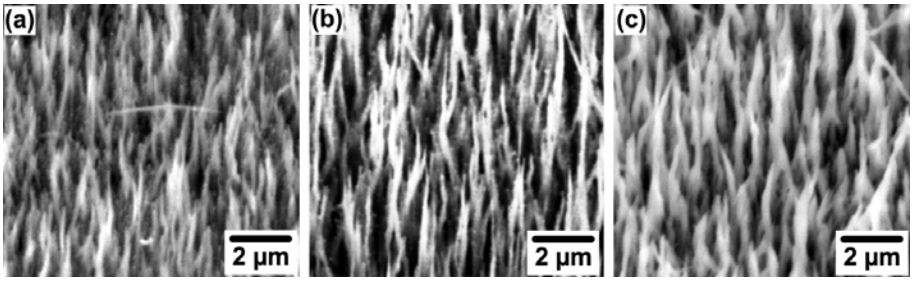

Fig. 21. SEM images of uncoated CNTs (a), 50nm nickel coated CNTs (b), and 100 nm barium strontium oxide coated CNTs (c). (Tilted 45° view).

The field emission measurement results are shown in Fig. 22. Fig. 22(a) contains the I-E plots showing the dependencies of field emission current on electric field for the CNT emitter and the oxide coated CNT emitter. The benefit of the low work function oxide coating can be clearly seen in Fig. 22(a). The field emission of the oxide coated CNT emitter was approximately 23.6 μA at 4.4V/μm, more than twice that of the uncoated CNT emitter. Fig. 22(b) shows the Fowler-Nordheim (FN) plots for the two emitters. The β factors for these two emitters were calculated from the slopes of the F-N plots. The work function values used for the calculation were the measured values of 1.9 eV and 4.5 eV for the oxide coated CNT emitter and the CNT emitter respectively. A fairly large β of 1484 was obtained for the CNT emitter, and a smaller yet still significant β of 467 was obtained for the oxide coated CNT emitter. This reduction of the β factor was a result of the increase of tube diameter due to the oxide coating. Field emission is described by the Fowler-Nordheim equation:

$$J = \eta a \frac{(\beta F)^2}{\phi} \exp(-b \frac{\phi^{3/2}}{\beta F}) \qquad (3)$$

where J is the current density in A/cm^2; ϕ is the work function in eV; a = 1.54 x 10^{-6} A eV V^{-2} and b = 6.83 x 10^7 (eV)$^{-3/2}$ V cm^{-1}; η is a factor that describes the geometrical efficiency of electron emission; β is the field enhancement factor; and F is the macroscopic electrical field in V/cm. As one can see from equation 1, field emission is very sensitive to the β factor. Given this strong dependence, a decrease in β of this magnitude would normally have resulted in a significant reduction of field emission

current. However, the work function is also a key factor that determines the field emission from an emitter. In this particular example, the lowering of the work function from 4.5 eV to 1.9 eV overcame the effect of the reduction of β from 1484 to 467, resulting in an overall increase of field emission.

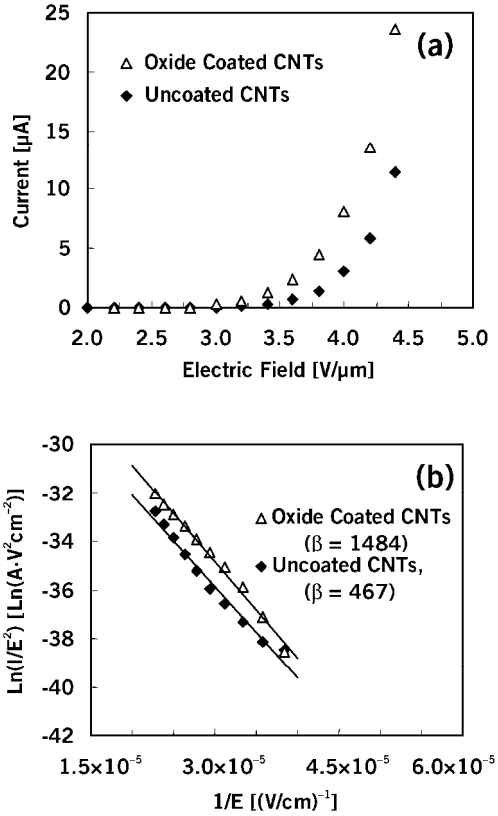

Fig. 22. Field emission current as a function of electric field, comparing emission from the uncoated CNTs to oxide coated CNTs (a), and the corresponding Fowler-Nordheim plots (b).

The governing equation for thermionic emission is the Richardson-Dushman equation:

$$J_s = 120T^2 e^{-11605\varphi/T} e^{4.4\sqrt{E}/T} \qquad (4)$$

where the term J_s indicates that this equation refers to the saturation current; T is the temperature in Kelvin; ϕ is the work function in eV; E is the external electric field in V/cm; and A is Richardson's constant, with a value of 120 A/K^2cm^2. The second exponential term in the equation represents the field effect in thermionic emission and is referred to as the Schottky effect. The first exponential and the preceding constants are called the zero field emission:

$$J_0 = 120T^2 e^{-11605\varphi/T} \qquad (5)$$

The determining factors for the thermionic emission are temperature and work function. The Schottky effect is usually not very large. However, a much larger field effect is possible by introducing a large field enhancement factor, which could potentially lead to

a dramatic increase in thermionic emission. Fig. 23(a) and (c) show the thermionic emission current density dependencies on electric field at various temperatures for the CNT emitter and the oxide coated CNT emitter respectively. Fig. 23(b) and (d) contain the corresponding Schottky plots for the CNT and oxide coated CNT emitters. Compared to the CNT emitter, the oxide coated CNT emitter produced thermionic emission at a much lower temperature. As predicted by the Schottky law, the emissions entered the saturation region at high electric fields and became linearly dependent on the square root of electric field for both the CNT and oxide coated CNT emitters. The zero field emissions at different temperatures were extrapolated and determined from the Schottky plots, which were then used to generate the Richardson plots. The Richardson plots for the CNT and oxide coated CNT emitters in Fig. 39(e) fit straight lines well, and the work functions of the samples were calculated from the slopes of the lines. The calculated work function value was 1.9 eV for the oxide coated CNT emitter and 4.5 eV for the CNT emitter, confirming a significant reduction of the work function due to the BaO/SrO thin film surface coating. The benefit of the low work function oxide coating is clearly demonstrated in the thermionic emission current density plots in Fig. 23(a) and (b). The thermionic emission from the oxide coated CNT emitter was more than four orders of magnitude higher than the thermionic emission from the uncoated CNT emitter. This jump in emission current and emission current density was the result of reducing the work function from 4.5 eV to 1.9 eV. At 1221 K and an electric field of 1.1 V/μm, a 14.6 mA emission current was obtained from the oxide coated emitter in constant DC operation mode. The area of the emission surface was 0.012 cm^2. An emission current density of 1.22 A/cm^2 was calculated based on the emission current and the emitting area. The emission current density of this magnitude at this modest temperature is among the best oxide cathodes ever reported.

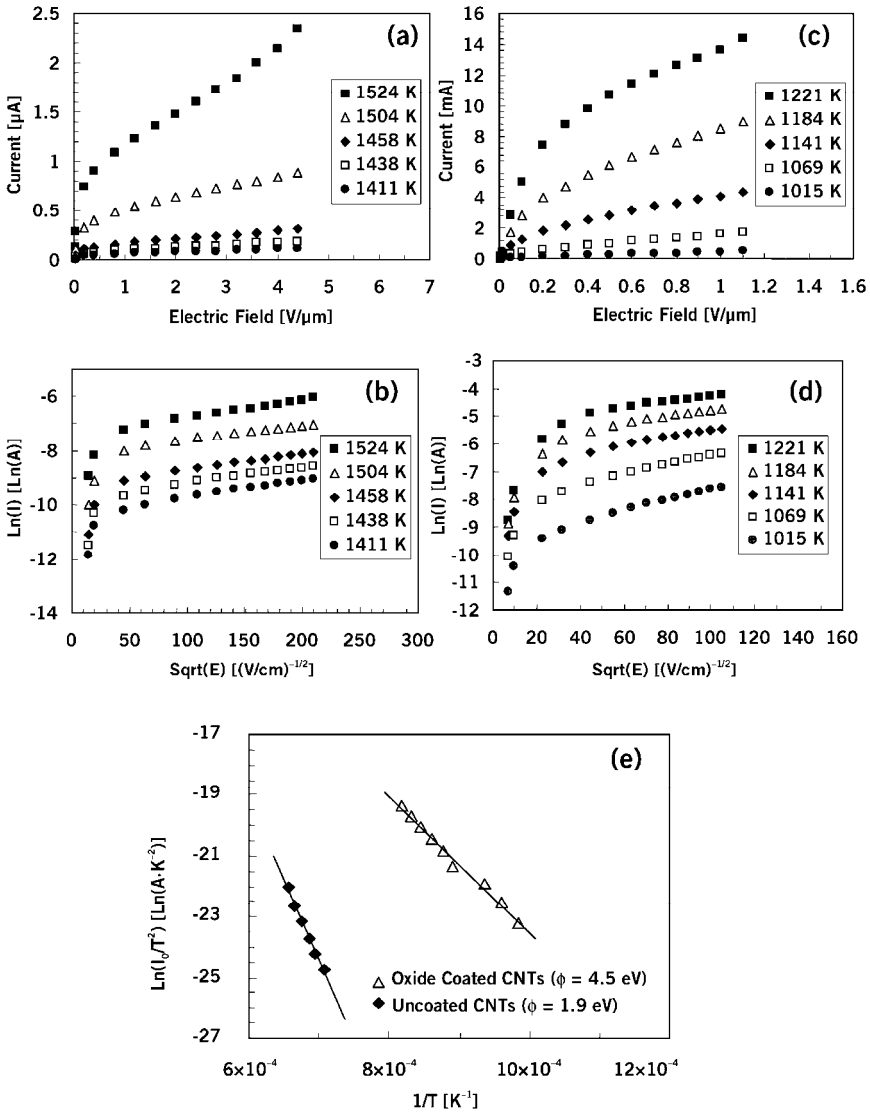

Fig. 23. The field dependence of thermionic emission current at various temperatures for the CNT emitter (a), the corresponding Schottky plots for the CNT emitter (b), the field dependence of thermionic emission current at various temperatures for the oxide coated CNT emitter (c), the corresponding Schottky plots for the oxide coated CNT emitter (d), and the Richardson plots for both the oxide coated CNT and uncoated CNT emitters (e). The work functions calculated from the Richardson plots are 4.5 eV for the CNT emitter and 1.9 eV for the oxide coated emitter.

The benefit of the low work function coating on the CNT surface was clearly demonstrated by the field and thermionic emission from the oxide coated CNTs. The barium strontium oxide coating reduced the work function of the emitter significant from 4.5 eV for the uncoated CNT emitter to 1.9 eV for the oxide coated CNT emitter. In the field emitter case, the overall field emission from the oxide coated CNTs was 2 times greater than that of the uncoated CNTs. Considerable room remains to improve the work function of the oxide coating. It is also possible to limit the reduction of β due to the

oxide coating by developing a thinner and more uniform coating. A robust surface coating based on oxide or other suitable low work function materials could potentially address stability and degradation issues surrounding CNT field emitters, and further extend their applicability to plasma and gas discharge devices. In the case of thermionic emission, the emission current from the oxide coated CNT emitter was more than four orders of magnitude higher than that of the thermionic emission from the uncoated CNT emitter. At 1221 K and an electric field of 1.1 V/μm, a 14.6 mA emission current and 1.22A/cm^2 emission current density were obtained from the oxide coated emitter in CW operation mode.

We have performed a large number of experiments to improve the emission from the oxide coated cathodes. We will use the following example to further illustrate the benefit of introducing CNTs into the oxide cathode. Here we compare the emission properties of three sample cathodes, No.1 the CNT cathode, No. 2 thin film oxide cathode, and No. 3 thin film oxide coated CNT cathode. Figure 24(a), (b) and (c) show the thermionic emission current density dependencies on electric field at various temperatures for the CNT cathode, the oxide cathode and the oxide coated CNT cathode, respectively. Figure 24 (d) has the corresponding Richardson plots for the oxide cathode and the oxide coated CNT cathode. The Richardson plots for the oxide and oxide coated CNT cathodes in Fig. 24(d) fit straight lines well, and the work functions of the samples were calculated from the slopes of the lines. The calculated work function values were 1.91 eV for the oxide cathode and 1.89 eV for the oxide coated CNT cathode, confirming a significant reduction of the work function due to the BaO/SrO thin film surface coating. The benefit of the low work function oxide coating is again clearly demonstrated in the thermionic emission current plots in Fig. 24(a) and (c). The thermionic emission from the oxide coated CNT emitter were more than two orders of magnitude higher than the thermionic emission from the uncoated CNT emitter. This jump in emission current and emission current density was the result of reducing the work function from 4.5 eV to 1.9 eV. At 1122 K, a 21-mA emission current (the current limit of our instrument) was obtained from the oxide coated cathode in CW operation mode. The area of the emission surface was 0.012 cm^2. An emission current density of 1.8 A/cm^2 was calculated based on the emission current and the emitting area. This is the best sample we obtained so far. The emission current density of this magnitude at this modest temperature is also among the best thermionic cathodes ever reported . Also apparent from the plots in figure 24 (b) and (c) is the benefit of high field enhancement factor introduced by the CNTs. The oxide coated CNT cathode had a similar work function as the oxide cathode. However, the thermionic emission from the oxide coated CNT cathode at equivalent temperatures was much stronger. For example, at approximately 1092 K, the oxide coated CNT cathode had emission current of 15.6 mA, more than ten times stronger than the emission of the oxide cathode at 1099 K. While in some applications, high emission current densities may be desired. In others, such as fluorescent dimming applications, it will be useful to introduce a means of reproducing the emission capability of a conventional oxide cathode at a lower temperature. Comparing Figure 24 (b) and (c), one can see that the oxide coated CNT cathode was capable of producing the same amount of current at a temperature 150 K lower than the oxide cathode. This is a significant improvement. To

put it into perspective, the temperature of a typical fluorescent lamp cathode changes between 100 K and 300 K in the whole dimming range.

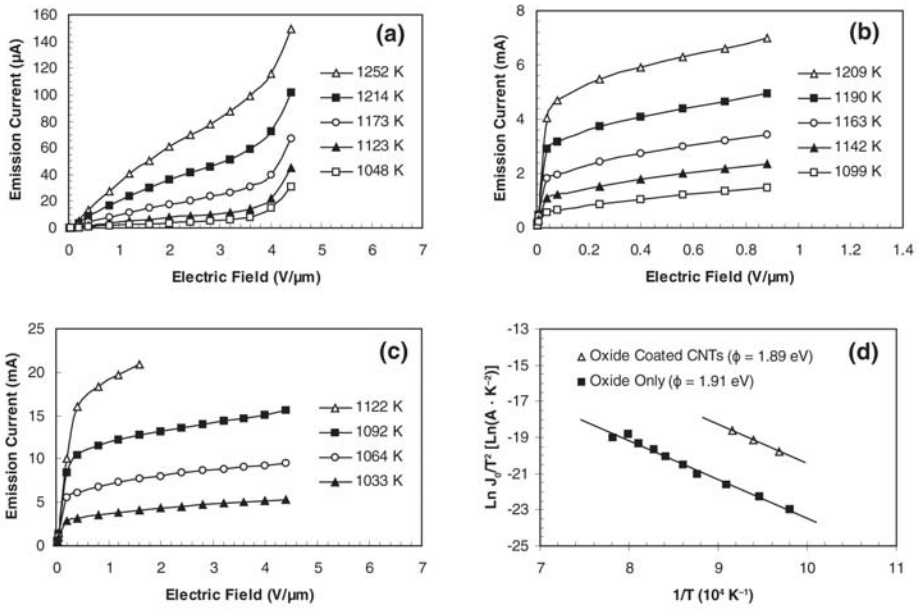

Figure 24. The thermionic emission of the CNT and oxide coated CNT cathodes: the thermionic emission current dependencies of electric field at various temperatures for the CNT cathode (a) the oxide cathode (b) and the oxide coated CNT cathode (c); and the corresponding Richardson plots for the oxide and oxide coated CNT cathodes (d).

It is important to stress that the emission current density of the oxide coated CNT cathode reported here is one of the best (if not the best) ever reported. A conventional fluorescent cathode typically operates at a current density approximately several hundreds mA at about 1300 – 1400 K. The oxide coated CNT cathode we created had a much higher current density at a much lower temperature. Use our earliest results presented in figure 3 as an example, the oxide coated cathode there is a typical fluorescent cathode and it had a emission current of about 2 mA at 915 ^{o}C (1188 K). The area of the emitting surface of the cathode is approximately 0.05 cm^2. Therefore, the current density for that fluorescent cathode is approximately 40 mA/ cm^2 at 915 ^{o}C (1188 K). Using the results from figure 3 and figure 30, table 3 gives a comparison between the emission current densities of the conventional fluorescent cathode, the thin film oxide cathode, and the thin film oxide coated CNT cathode. It can be estimated that at comparable temperatures, the emission current density of the oxide coated CNT cathode has improved by approximately two orders of magnitude compared to the conventional fluorescent cathode.

There remains significant room for further improvement. For example, the work function for the thin film oxide coating is around 1.9 eV, which is relatively high compared to much lower work function values (~ 1.5 eV) obtained in some other experiments. With further improvement in fabrication techniques, it is likely that we will

be able to further reduce the work function value for the oxide coating for the CNTs. The key challenge here is to reduce the work function of surface coating and at the same time introduce a large field effect.

Table 3: Comparison of emission from different cathodes

	J (mA/ cm^2)	T (K)	Work function (eV)
Fluorescent cathode	40	1188	2.0
Thin film oxide Cathode	400	1190	1.9
Thin film oxide coated CNT cathode	1800	1122	1.9

There were samples that shown significant lower work function and even stronger emission. Although more work need to be done to improve the process and thus to reliably reproduce those samples, they at least demonstrated the potential and possibility for super-efficient cathodes that can operate at much lower temperature. Figures 25 and 26 show one of these samples that has extraordinary large emission. The emission current used in these figures is Ampere (A). Also notice that the emission area of this prototype cathode is much smaller then a typical fluorescent cathode yet the emission current is compatible to that from a typical fluorescent cathode.

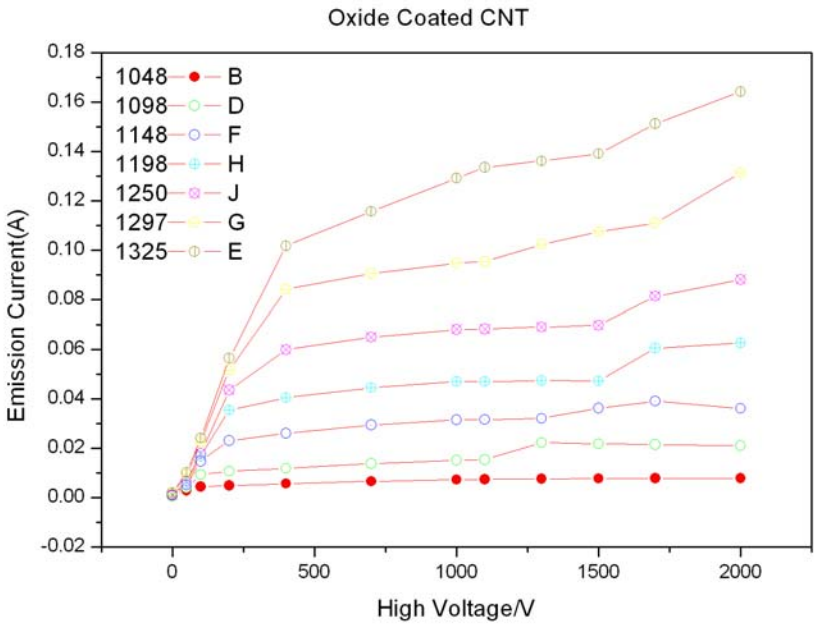

Figure 25. Oxide coated CNT with $\varphi = 1.06$ eV

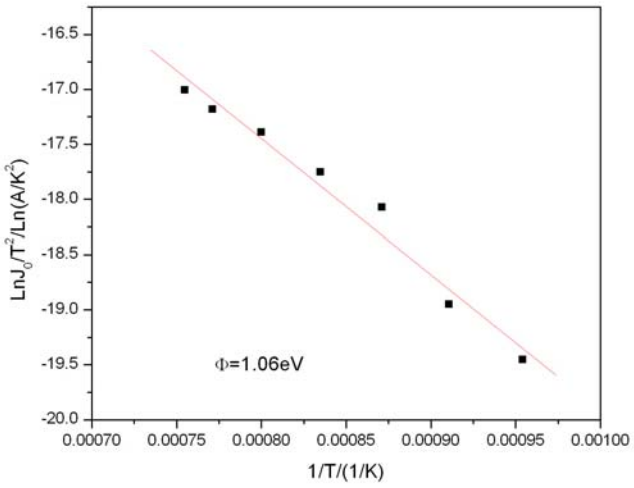

Figure 26. Work function measurement for the experiment corresponding with Fig. 30.

E. Electron Emission Measurement Techniques and Characterizations of Emission of Prototype Cathode in Vacuum

A customized electron emission measurement system was used to characterize the electron emission properties. Both the initial design (DC measurement) and the improved design (Pulse measurement) are described in this section.

The system we have is capable of measuring electron emission current from a cathode at different temperatures, different field strengths, as well as the work function of materials. The measurement is performed in a UHV environment at 10^{-9} torr residual pressure. This system has a RGA attachment and is capable of performing in-situ cathode activation process.

The cathodes were placed in the chamber in simple diode configuration. The cathodes were installed on two copper rods that fed through to the outside of the vacuum chamber. A voltage was applied across the copper rods to resistively heat the cathode by flowing a current through. An Agilent E3631A source meter was used to provide this voltage. The anode consisted of a copper plate mounted on a linear motion feedthrough. The distance between the anode and the cathode could be established to the nearest thousandth of an inch (0.025 mm) using the feedthrough. A high positive voltage was applied to this plate using an electrical feedthrough that connected the plate directly to a power supply. A Keithley 2410 source meter was used to provide this high voltage, and to measure the emission current. This meter had an upper limit of 1100 V and 20 mA, which formed the ceiling for most of the data presented in the next chapter. A Glassman power supply with limits of 4000 V and 4 A was also used to provide the high voltage, using a Keithley 2700 multimeter to measure the emission current. This configuration was implemented close to the end of the study, so only a small amount of the data

presented in the next chapter were extracted using this system. The circuit is shown in Fig. 27 along with a diagram of the measurement system.

The temperature of the cathode was measured using an optical pyrometer. The pyrometer contains an adjustable, calibrated filament. When looking through the eyepiece, the filament is superimposed over the image that is observed through the lens. By superimposing the pyrometer filament over the cathode, it is possible to measure the temperature of the cathode by adjusting the pyrometer filament until it is the same color.

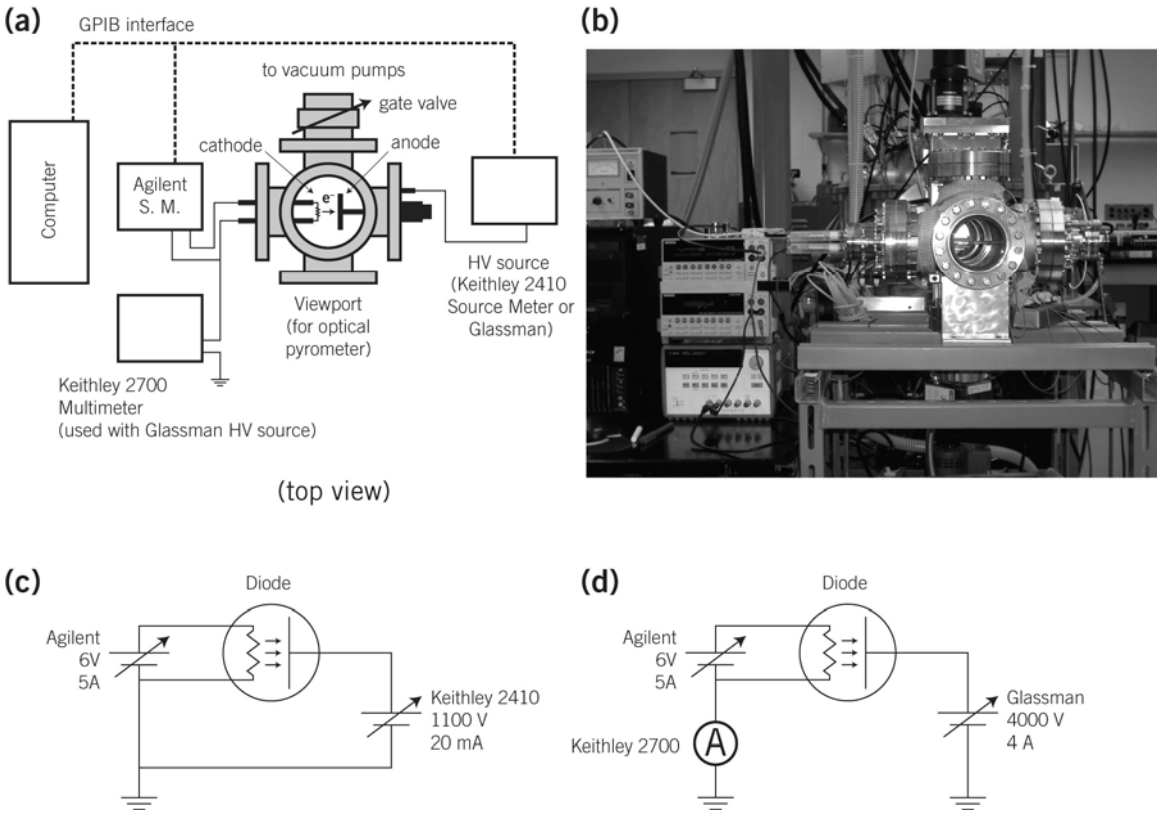

Fig. 27. A diagram (a) and photograph (b) of the electron emission characterization chamber; and circuit diagrams showing the use of the source meter with internal ammeter (c) and high voltage power supply with external ammeter (d).

The temperature can also be calculated using the change in the resistance of the cathode. The room temperature or "cold" resistance is measured using a four-wire resistance measurement prior to the measurement process, while the resistance during cathode heating is computed using Ohm's law and the voltage and current measured by the Agilent source meter. It is possible to calculate the temperature using these data by the following formula:

$$\Delta T = \frac{1}{\alpha}\left(\frac{R_H}{R_C} - 1\right) \tag{6}$$

where α is a constant related to W, with a value equal to 4.505×10^{-3} K^{-1}.

For oxide coated cathodes, cathode activation was required before the emission measurements could be taken. Because of exposure to air, unwanted material was adsorbed on the surface of the cathode, such as water vapor. It was necessary to first heat the cathode to purge the surface of these materials. The field emission from fully activated cathodes was found to be much greater than that of unactivated cathodes.

Two measurement procedures were used, one to measure the field emission, and another to measure the thermionic emission. The field emission measurement collected the room temperature emission current of the cathode at varying anode voltages. From this data it is possible to extract information such as the turn-on voltage, which is defined as the voltage at which the emission current rises above an arbitrary value. The Fowler-Nordheim (F-N) equation was applied to determine the field enhancement factor (β) of the cathode surface.

The thermionic emission measurement was used to determine ϕ. The emission current was measured from the cathode at varying anode voltages, at different cathode temperatures. Each data set was used to produce one Schottky plot, producing one value for the zero field emission for each temperature. These were used to produce a Richardson plot using the logarithm of Eq. 5. with constants in place,

$$\ln \frac{J_0}{T^2} = -11605 \frac{\phi}{T} + \text{const.} \qquad (7)$$

where a plot of $\ln J_0/T^2$ versus $1/T$ is the Richardson plot, and the slope of this line is proportional to ϕ by -11605 $(\text{eV}\cdot\text{K})^{-1}$.

The field emission measurement is used to measure β. Unlike the thermionic emission measurement, in which the temperature must be determined visually, the field emission measurement can be fully automated. The Keithley 2410 source meter was equipped with a general purpose interface board (GPIB) connection, which was used to remotely control the instrument. A program was written in LabView to collect the field emission data. To produce the F-N plot, the logarithm of the current was taken, and each data point was divided by the square root of the electric field at which it was collected. The electric field was determined in the same method as with the thermionic measurement. It is the slope that is of interest in the determination of β. According to Eq. 3, the slope of the F-N plot is proportional to $\phi^{3/2}\beta$ by -6.82×10^7 $\text{eV}^{3/2}\cdot\text{V}\cdot\text{cm}^{-1}$. Therefore, it is possible to calculate β using the following formula,

$$\beta = \frac{\left(-6.82 \times 10^7\right)\phi^{3/2}}{\text{slope}}$$

A large number of cathodes and their field emission and thermionic emission were measured using this system with the above described methods.

During the first two years of this project, the power supply that we used has a current limit of 20 mA and that's the reason that the results shown in the earlier section all have emission current less than 20 mA. However, the emission currents from our

prototype cathodes were actually much larger, and we had to limiting the cathode emission area and temperature in order to accommodate our measurement system. The very strong emission from our cathodes presented a unique challenge to our experimental technique. Because of the strong electron emission from our cathode, the anode which receives electrons became over heated to a very high temperature and which in turns becomes an electron emitter. This put a significant limit on the level of electron emission that could be measured in our earlier system. To resolve the issue, a significant amount of effort was devoted to improve the thermionic technique and measurement system. Figure 28 is a sketch of the improved thermionic electron emission characterization system based on the pulsed measurement technique.

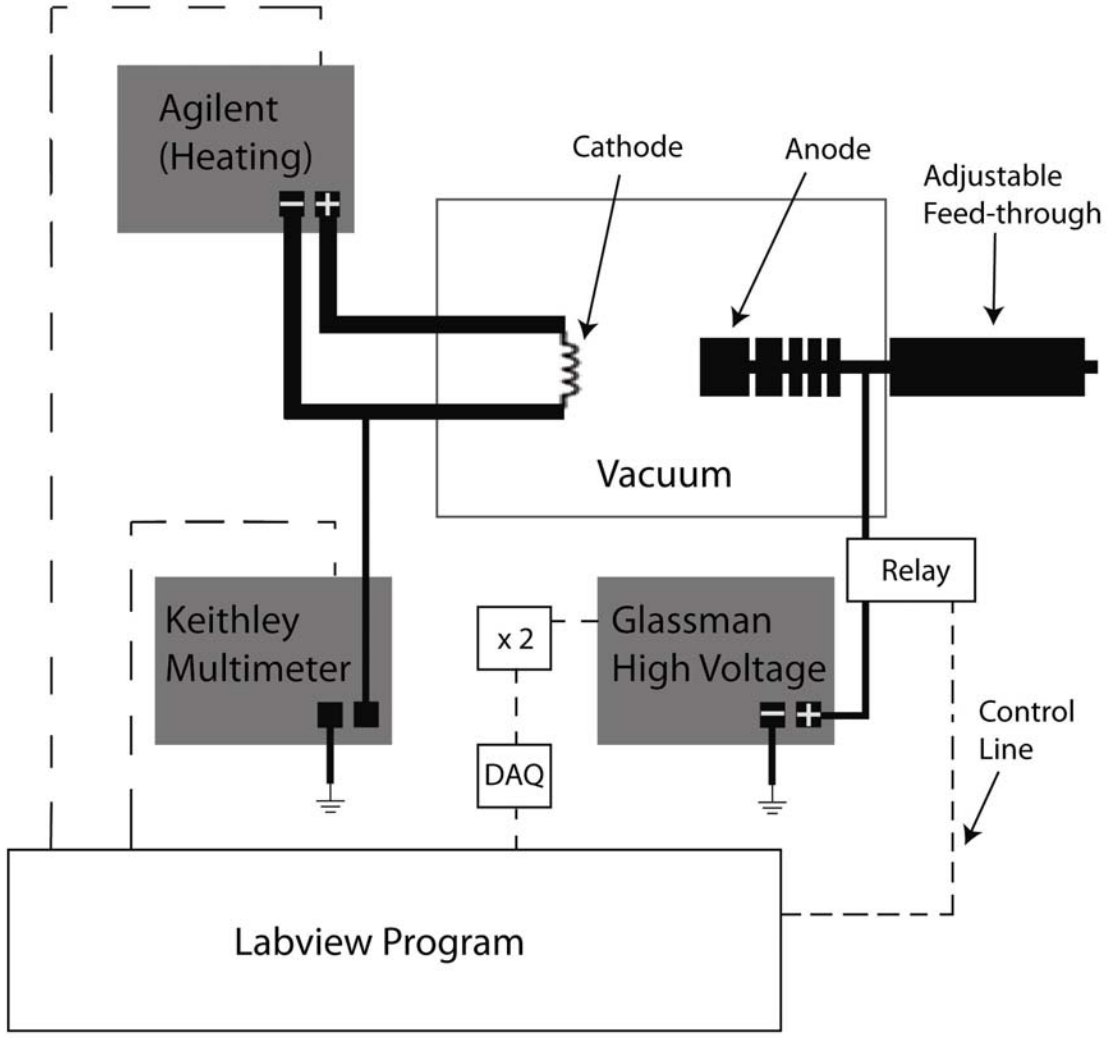

Fig 28. Schematic of current experimental setup.

X2 is the op-amp circuit that doubles the voltage signal to the Glassman. This is done because the Glassman requires a voltage 0-10 V as a signal to control the corresponding high voltage output 0-5000 V. DAQ is the Data AQuistion USB board that sends a voltage to the Glassman. The Keithley multimeter reads the emission current

from the circuit and is interfaced to Labview using an IEEE GPIB interface. The Agilent power supply is also interfaced using an IEEE GPIB interface. The relay is used to rapidly switch the high voltage on and off.

There are several unique features about this improved system. First of all, the anode was designed to be an effective heat sink itself by being large in mass and by having a larger surface area to improve thermal conduction and the blackbody radiation, respectively. Furthermore, a pulse measurement method was developed to significantly reduce the amount of time that anode receives electrons, thus reduce the heating. This was done by using a controllable relay to regulate the Glassman high voltage source. This measurement scheme not only allowed higher emission current to be measured but also reduced sparking, which was destructive to the cathode, and thus produced more accurate measurement results.

The overall measurement and data collection was controlled by a LabView program. The control front panel and block diagram of the control program are included in the appendix. In this measurement, the cathode was placed in an ultrahigh vacuum chamber in a diode configuration as shown in Fig. 4.1. To set the cathode temperature, a small voltage was applied by an Agilent E3631A source meter between the two ends of the cathode to create heating on the surface of the cathode via resistance of the cathode substrate. A cylindrical copper anode was placed opposite of the cathode to collect the emitted electrons by applying a bias voltage supplied by the Glassman High Voltage power supply. The distance between the anode and the cathode could be changed by an adjustable feed-through attached to the anode. This distance when used in conjunction with the high voltage supply could create the desired electric field. Due to vacuum limitations, the distance between the cathode and anode had to be increased because the high fields created in such a short distance caused some sparking which was damaging to the cathode. The electron emission current at various field strength was then read by a Keithley 2700 multimeter. This process was repeated at various cathode temperatures. A LabView 8.0 program was written to collect emission current data associated with a given heating temperature and a set of high voltages.

As a result of improving the diode system configuration (i.e. pulse measurement, larger anode, automation, etc.) we were able to measure a much larger emission current that was off the limit previously with the DC measurement technique. For example, figure 29 shows a typical sample cathode that we created recently. An emission current as large as 210 mA was observed. Such strong emission level was not possible to be measured prior to the improvement, and such strong emission promises many potential practical applications for this new cathode.

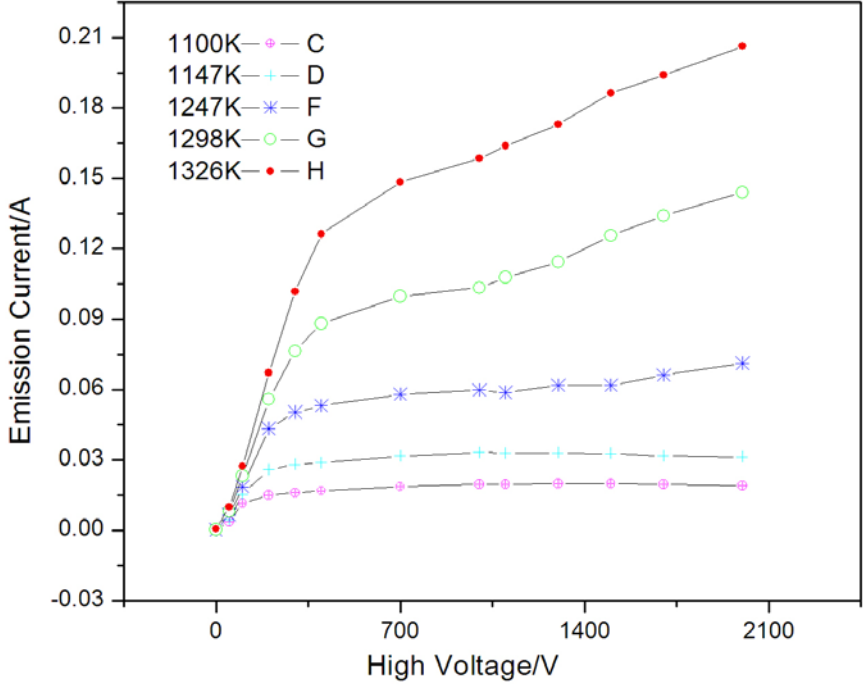

Figure 29. Oxide coated CNT cathode with very strong emission measured with the pulse method.

Future cathodes and variants of the oxide coated CNT prototype cathodes may produce a current even larger than what has been observed. As previously mentioned, the vacuum pressure is an important factor when making an emission current measurement in an ultrahigh vacuum because destructive sparking may occur if the pressure is too large. An ion pump has been employed to address this problem as it is able to maintain a vacuum around 10^{-9} torr. Plus, with every emission, there is an associated sputtering or evaporation that made the pressure rise and cause subsequent sparking on the cathode. Two ways to address this problem is to increase the distance between the anode and cathode or to wait a longer amount of time in between measurements. Increasing the distance between the anode and cathode can also be a problem because more voltage is required to maintain the same electric field, plus the electrons accelerated to the cathode will have much higher energies that might cause some electron scattering on the anode causing the electrons not to be observed as emitted current from the cathode.

E. Thermionic Cooling Phenomenon

Another effect that we studied during the course of this project is also worth reporting. When measuring emission currents from samples with strong emission at higher temperatures, a peculiar phenomenon was observed unexpectedly, at higher current, emission current decreases as field or bias high voltage between the anode and cathode increases. Following is a typical result that we obtained, as we can see in this particular case, emission current exceeds 26 mA even at modest bias voltage but start to decrease as bias voltage increase, which reverses the expected trend completely.

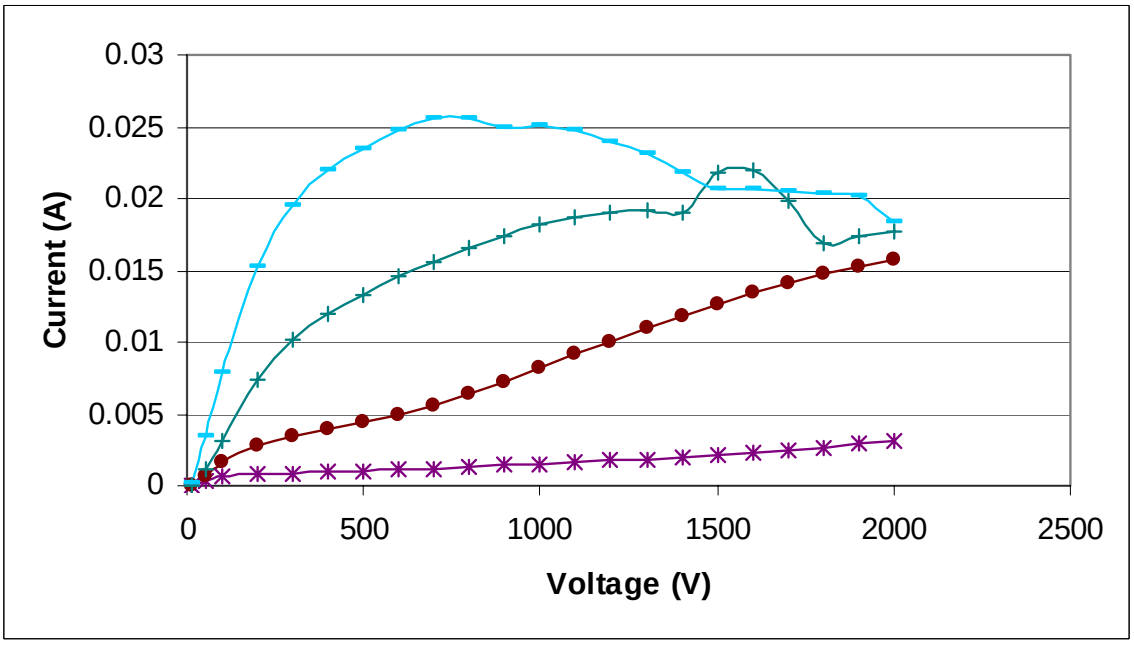

Figure 30. Emission at high cathode temperature drops as bias voltage increases.

Our explanation of the observed the phenomenon is that at high emission current, there are large amount of hot electrons emitted from the surface of the cathode and these hot electrons carry away significant amount of energy from the surface and thus cool the cathode surface to a lower temperature. And as a result of this cooling effect, the emission from the surface drops. As we will discuss later this cooling effect is significantly large due to the strong emission from our prototype cathodes and could be useful in both thermionic cooling and energy conversion.

The concept of thermionic energy conversion and cooling has long existed. Thermionic cooling was proposed to improve the Carnot cycle of heat engines or provide cooling for semiconductor devices among many other potential applications. While there is still a long way to go to develop practical thermionic energy conversion devices with broad applications, devices based on such concept do exist. For example, thermionic emission has even been employed in solar thermionic converters. These solar converters focus the light into one concentrated area to produce a high temperature that can be used for thermionic energy conversion. One reason that hindered the development of this type of solar energy converter and other thermionic devices is the lack of low work function materials that can create a large current. The oxide coated carbon nanotube emitter, however, exhibited large emission current, make it an excellent novel electron emitter that may be eventually used in applications such as thermionic cooling.

Thermionic cooling from a cathode can be achieved when the energy leaving the cathodes via electrons is greater than the energy of the electrons at the surface of the emitter. This energy difference between emitted and replaced electrons is called the energy exchange or Nottingham effect. The average internal energy of the conductor is called the chemical potential or μ. The Fermi energy, ε_F , and chemical potential are related approximately by:

$$\mu(T) \cong \varepsilon_F[1 - \frac{1}{12}\pi^2(k_B T / \varepsilon_F)^2 + ...]$$

When $\mu > \varepsilon_r$, the average replacement energy, then thermionic cooling can occur. At higher temperatures, there is more current from thermionic emission and μ becomes even more greater than ε_r. Therefore, the stronger the emission current or current density, the stronger the cooling effect.

We have preformed detailed measurements on temperature drop or thermionic cooling effect from our prototype cathode surface. In these experiments, the temperature drop due to electron emission was measured. The temperature of the cathode was raised by flowing a electric current through the tungsten foil and was measured at the center of the foil by means of a high temperature pyrometer. The bias voltage between the cathode and anode was controlled manually by the Glassman high voltage supply—capable of sustaining a voltage up to 5000 V. Current from electron emission was monitored by the Keithley current meter. To get more accurate results, a larger area was used as an electron emitter to minimize the effects of conductive temperature dissipation in the tungsten foil. The emission area was approximately 0.77 cm^2.

The cathode was mounted by two set screws as seen in Fig. 31 and heated to a temperature above 1000 ^oK, the lower limit of the optical pyrometer. Before the current emission measurement, the temperature was calibrated with the current—rendering an initial temperature measurement denoted T_o. One temperature measurement was considered to be the average of five individual measurements. The cathode was heated by manually controlling the voltage and current of the Agilent current source. A high voltage was applied to the anode by the Glassman High Voltage power supply via a LabView SubVI program. When the cathode was heated and a high voltage was applied, a temperature measurement was recorded. This measurement was recorded for various voltages at several (4-6) temperatures. The temperature was measured from the center of the cathode to minimize the error associated with heat dissipation through the tungsten foil.

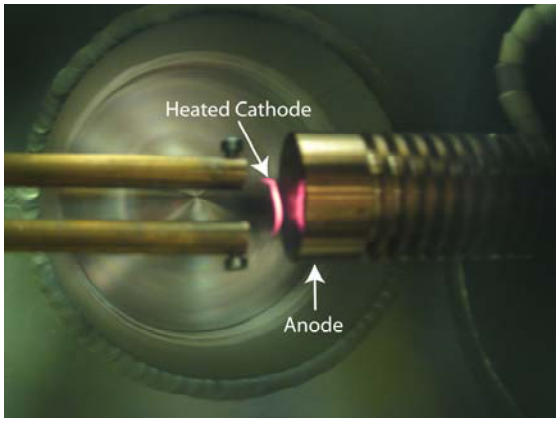

Fig 31**.** A heated cathode in the diode setup.

Up to a 90 degree Kelvin temperature drop was observed and Fig. 32 shows one of the samples measured.

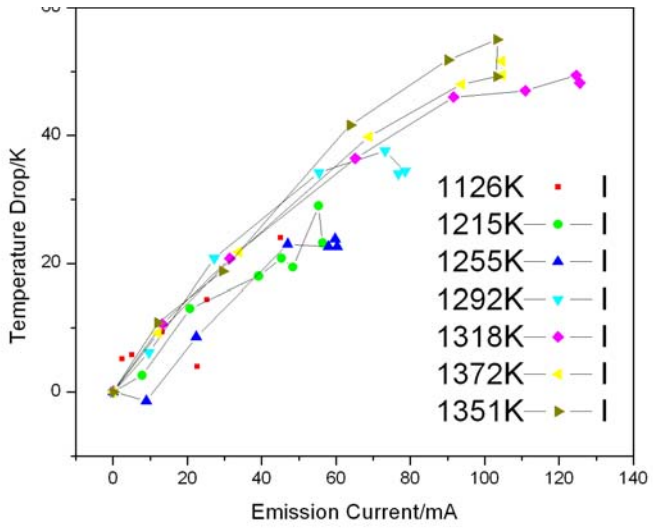

Figure 32. Temperature drop versus emission current. The temperature legend corresponds to the initial temperatures.

Towards the end of every temperature measurement set, the temperature drop did not continue to increase as the current increased. It is expected that the temperature drop should be proportional to the emission current regardless of the original temperature because an amount of emitted electrons should cause the same amount of cooling. One explanation for this deviation is that the temperature is being dissipated through the tungsten faster than it can be lowered by thermionic electron emission. The observed temperature drop is expected to increase if a tungsten foil with less width is used. The true temperature drop is estimated to be larger than what is observed because of this heat dissipation effect. A smaller tungsten foil substrate is expected to lower this dissipation by constricting the area in which the heat can be dissipated.

Such a large temperature drop was observed due to a large emitting current via thermionic emission. This temperature drop may be used in future applications to cool devices and create energy. The efficiency of thermionic energy converters continues to improve as the work function and emitting material is improved. Semiconducting heterostructures have also been used in an attempt to lower the work function in order to create thermionic cooling. Such devices may be coupled to other solid state devices to create cooling "on the chip." A device has been created in another laboratory to cool a computer chip much like a heat sink due to the increased area given by an array of CNTs. The cathode designed in this laboratory may be able to combine the effects of being a heat sink due to the use of CNTs and a good thermionic cooler to create a very good cooling device.

The emission current results are not limited to the temperature range measured in the lab. As shown in Fig. 32, the temperature drop is quite independent of the initial temperature that is measured. For example, if the initial temperature was 700 ^{o}K, then we would observe the same temperature drop as seen in Fig. 32. This allows for the introduction of many new applications. Many systems that operate in a moderate

temperature range, such as nuclear power plants and other machinery, could benefit from thermionic cooling.

F. Discharge Simulator and Prototype Performance in Plasma

Operating a cathode in a plasma environment can be much more difficult than operating in a vacuum environment, but it is essential to application in discharge devices such as fluorescent lamps. The discharge simulator that we constructed has many of the same constituents as a fluorescent lamp: an argon/mercury plasma environment, high frequency alternating current ballast, and a tubular design that resembles a fluorescent tube. Figures 33 – 35 are the sketch of the simulator and pictures of this simulator in operations.

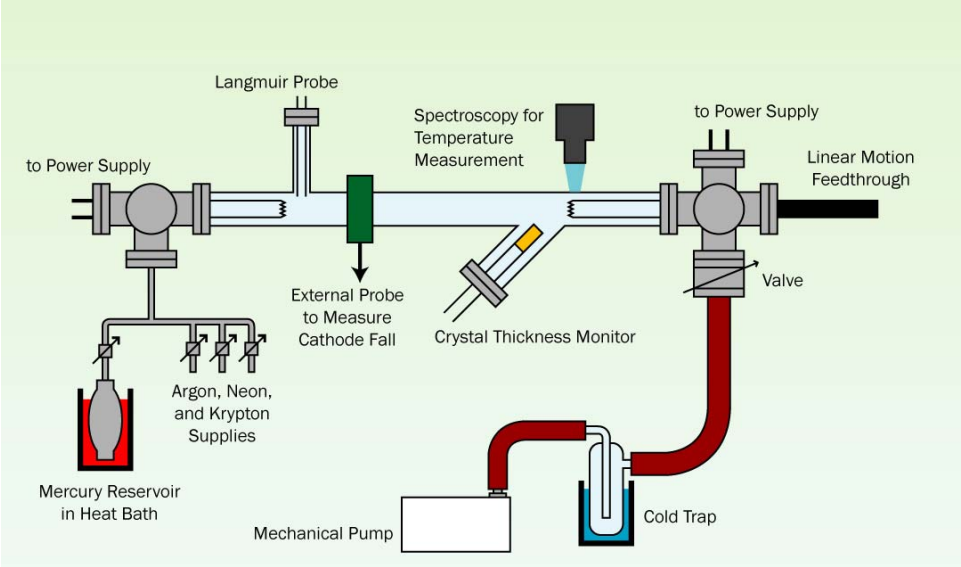

Figure 33: Sketch of the plasma discharge simulator

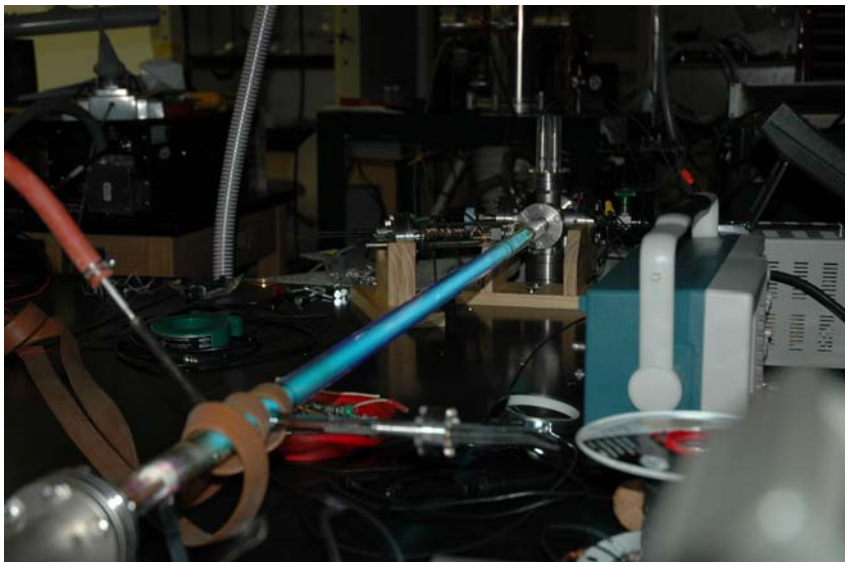

Figure 34: Plasma discharge simulator in operation.

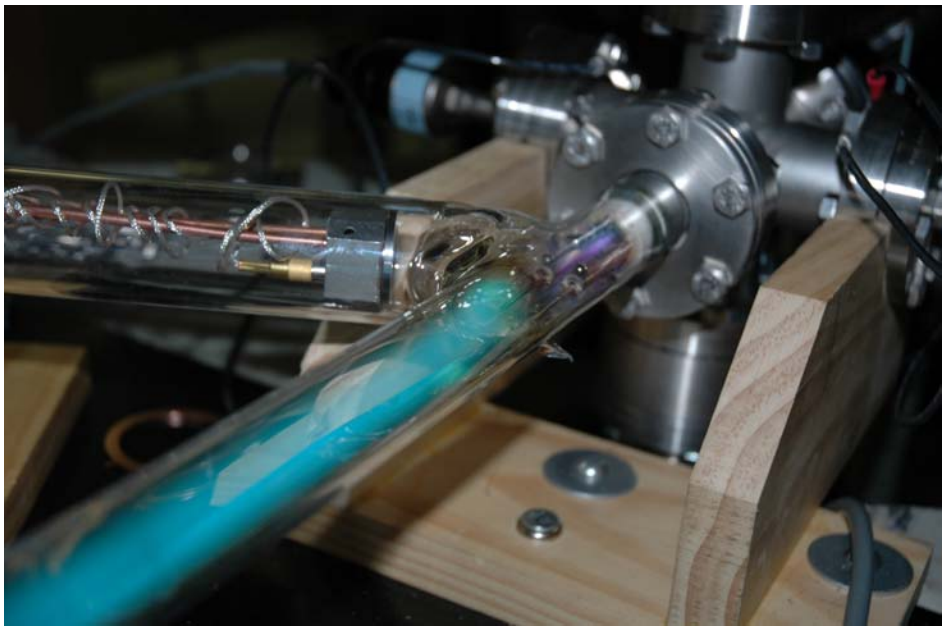

Figure 35: Plasma discharge simulator in operation- details around the cathode area. The side branch point to the cathode is the sensor of a sputter yield system.

Discharge lamps generally are powered by an AC current above at a frequency above 1 kHz . The AC current is supplied by an electronic ballast, in this case the Lutron Hi-Lume electronic dimming ballast. The ballast provides a high voltage between electrodes, allowing electrons to accelerate and create charged atoms of gas such as argon and mercury. The initial voltage across the entire lamp must be relatively large, but the operating voltage must be lowered after a plasma is established to limit the current so that the cathodes will not be damaged or destroyed. Simply, this is what the ballast does: it controls the amount of current going through the lamp at any given time. The fundamental ballasting effect can be thought to be caused by an extra resistor put in series with the circuit, a ballasting resistor, that has no effect on the open voltage between the anode and the cathode. When the circuit is closed, the resistor limits the current going through the entire circuit and reduces the operating voltage of the lamp by acting as a simple voltage divider, assuming that the plasma in the lamp has a given resistance. Actual ballasts, however, contain more electronics than just a ballasting resistor to control the current more precisely, but the overall effect is still the same.

In operating conditions, the lamp contains three main spatial regions inside of the lamp: the cathode fall, the positive column, and the anode fall. With our ballast operating at 50 kHz, the anode fall voltage is relatively small compared to the anode fall and the positive column. The positive column is what produces the useable ultraviolet light, which is converted into visible white light by a coating of phosphorous on the inner surface of tube in conventional fluorescent lighting. The cathode fall, however, produces very little visible light and has various effects on the cathode, therefore this is what is measured.

The positive column retains a positive voltage while the cathode is at a negative potential with respect to the discharge in the positive column. This potential difference between the cathode and the positive column is called the cathode fall. The cathode fall determines the electric field experienced by the cathode. A high cathode fall can lower the effective work function by the Schottky effect, but this is at the price of a high sputtering rate. A high sputtering rate, in turn, will decrease the lifetime of the cathode. Adding auxiliary heating to the cathode allows it to emit more electrons via thermionic emission. This too, however, can end a lamp's life prematurely by loss of material via evaporation.

To help a cathode emit more electrons themionically, barium, strontium, and calcium are used to lower the work function of the tungsten filament. This forms a semiconducting oxide layer, such as barium oxide, on the surface of the tungsten to help it emit more electrons for a given high temperature. The chemical process that is believed to occur at the interface of the tungsten and the barium oxide is such:

$$6BaO + W \rightarrow Ba_3WO_6 + 3Ba \quad .$$

The measurement setup in the discharge simulator resembles a fluorescent lamp with two tungsten filaments and in shape and in length of the tube. On each end of the lamp, there is a CF flange in which the cathode holder can be mounted (see Fig. 36).

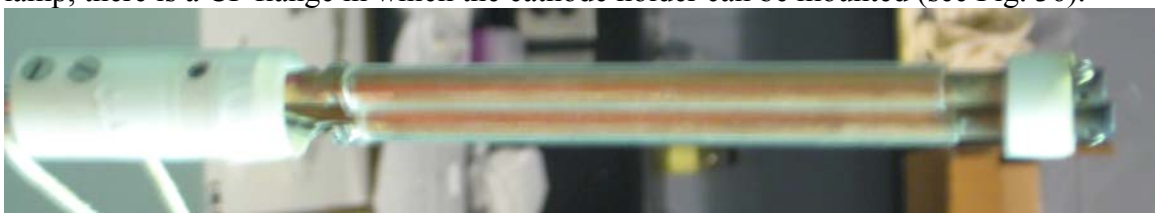

Figure 36. Discharge simulator cathode sample holder.

To prepare for the experiment, the cathode holders were removed from both sides of the lamp. On the non-adjustable cathode holder, a barium/strontium/calcium carbonate powder was dissolved in a solution of acetone or acetonitrile and then deposited on a tungsten coil. Once under a vacuum, the carbonate powder was turned into an oxide powder by activating it via a heating current. The test cathode, which might be a powder sample, an oxide layer, or a oxide coated CNT, was loaded on the adjustable end of the lamp. Once under a vacuum a small flow of argon gas was fed through the system to build a pressure of around 30-100 mTorr. Mercury was released into the lamp through the mercury supply tube. When a desirable pressure had been reached, the plasma was ignited.

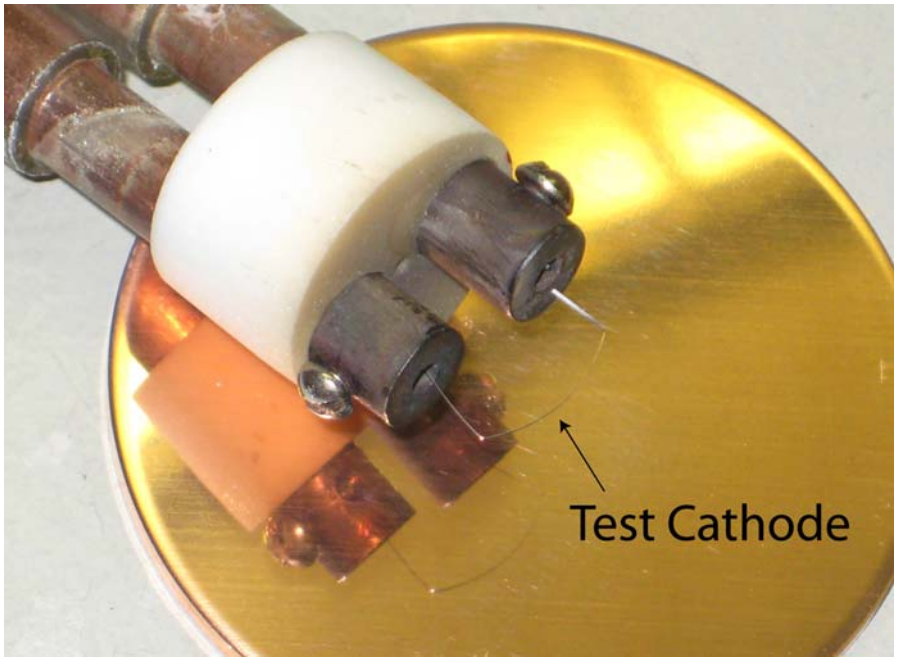

Figure 37. The discharge simulator test cathode holder and test cathode.

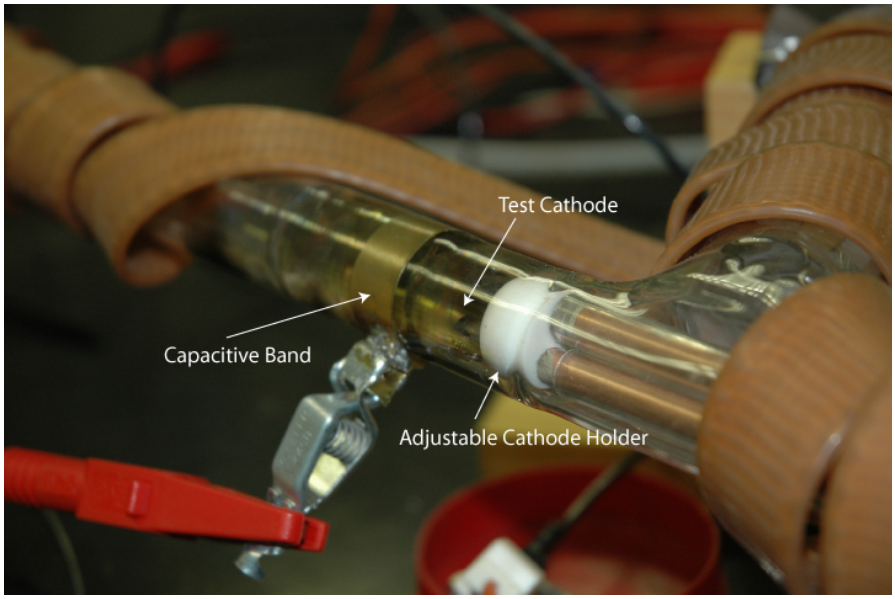

Figure 38. The discharge simulator testing apparatus.

Data collection was obtained by using a Tektronix TDS 3034B oscilloscope. When collecting data, there were several things that are measured: the operating voltage, the cathode fall via capacitive coupling, sputtering yield, sample cathode temperature via pyrometer, system pressure, and argon flow rate. The length between electrodes is also adjustable. When measuring this length against the operating voltage, the cathode fall can be obtained. A comparative cathode fall, however, could be obtained by measuring the voltage at the cathode by capacitive coupling, or the band method, by placing a small metal band near the cathode on the outside of the lamp. The other end of this

measurement is electrically connected to the cathode. The voltage difference measured between this and the metal band is called the cathode fall.

Under a good cathode, the lamp would light up with a strong (arc) discharge—this is when data was collected. When the cathode was not good or when the emitting material was used up, the lamp would drop down into a quasi-stable state in the glow discharge range. When the lamp was in an arc discharge mode, it could have a 200 mA system current, such as for the powder sample. If the peaks of the oxide powder and oxide layer samples are compared (Fig. 39 and Fig. 40), the oxide layer sample is slightly better than the oxide powder sample because it spans less voltage. The band was measured at the positive end and the test cathode as negative; so the test cathode worked as the actual cathode at the negative side of the cycle, which would be the lower half of the figures below.

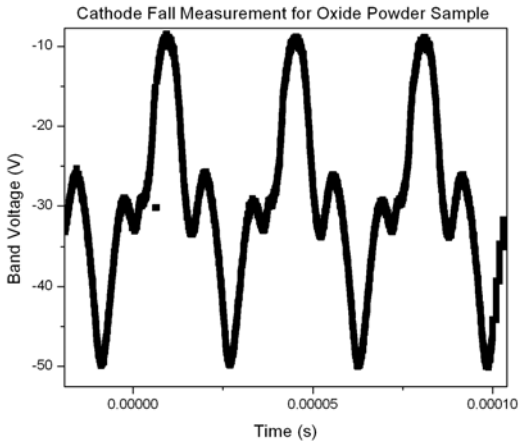

Figure 39. Band method measurement for an oxide powder cathode

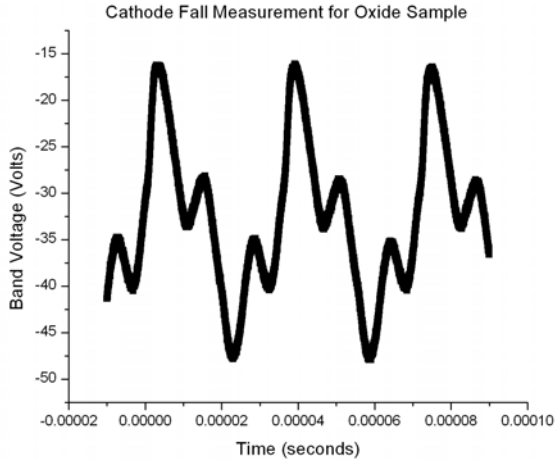

Figure 40. Band method measurement for an oxide film cathode

The oxide coated CNT sample worked well as a cathode in the glow discharge range, but would not enter the arc discharge range for very long because the emission materials were quickly used up. The oxide coated CNT tungsten foil had a higher conductivity than its oxide coated counterpart due to the conductivity of CNTs. Therefore, much heating current was necessary to get a sufficient heating temperature that was in the range of the optical pyrometer (1000 ^{o}K). An oxide coated CNT tungsten sample with a smaller width was then used in an attempt to remedy this, but after a few seconds in the arc discharge range, the emission materials were quickly sputtering off of the sample and the plasma returned to the glow discharge range.

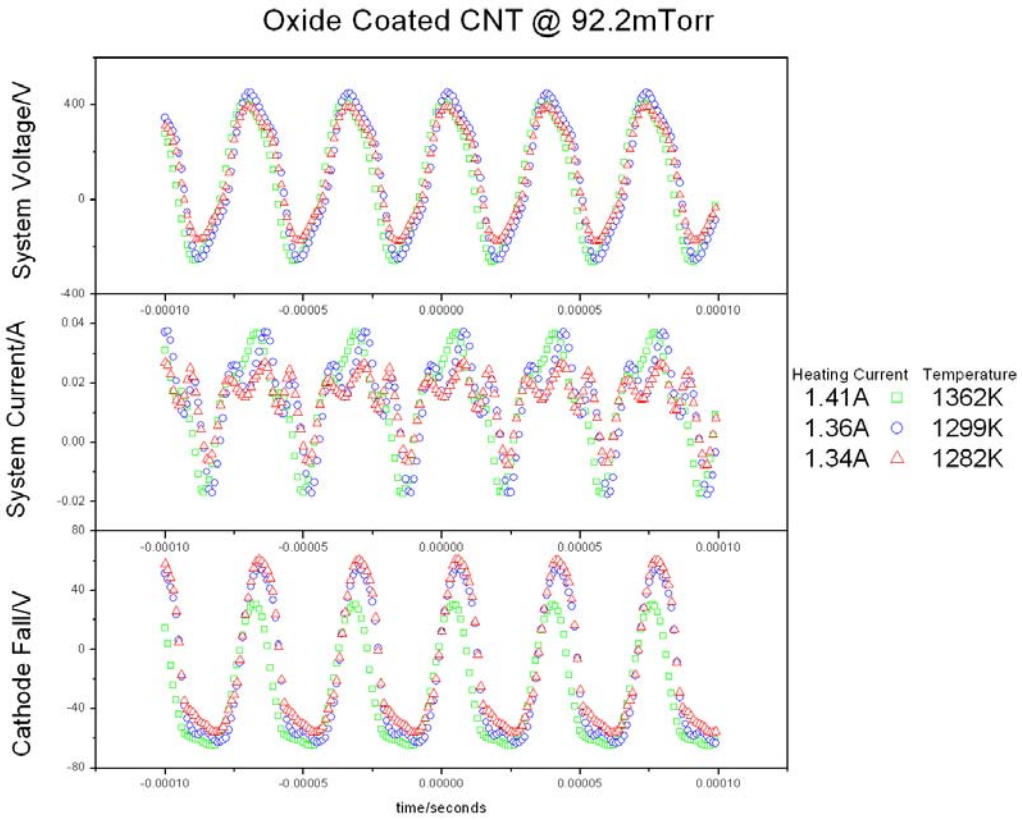

Figure 41. Oxide coated CNT sample demonstrating the lowering of cathode fall with an increase in heating temperature

Fig. 41 demonstrates how a cathode fall measurement can be used to compare the effectiveness of a cathode. As the cathode is heated, it is able to emit more electrons thermionically and ultimately achieve a higher emission current. As previously mentioned, the ballast is trying to maintain a constant system current, so what was observed is a drop in the necessary electric field to produce this consistency in current. Therefore, as the necessary electric field across the cathode drops, the corresponding voltage fall will drop.

Testing a cathode in a plasma environment presents many challenges—some expected and some undesirable, but is considered a necessary hurdle to overcome if some

of the desired applications are to be realized, such as a fluorescent lamp. It is considered a major success to be able to build a cathode and have it illuminate a constructed lamp under the right system conditions and parameters—all in one laboratory. The discharge simulator has many of the same characteristics of the fluorescent light bulb: an argon/mercury plasma environment, high frequency alternating current ballast, and a tubular design that resembles a fluorescent tube.

One of the related problems regarding the CNT cathodes is how do they age at high operating temperature required by fluorescent lighting. We have conducted some primary studies on thermal degradation of CNTs. The results seem to suggest that the emission properties of CNTs remain largely unchanged even after thermal treatment at temperature significantly above normal fluorescent cathode operating temperature. Figure 42 shows SEM images of an untreated CNT sample, and two CNT samples thermally treated at 800 ^{o}C and 1200 ^{o}C. It was found that the morphology of the CNT sample after thermally treated at 800 ^{o}C remained largely unchanged. But there was a noticeable change in morphology for the sample treated at 1200 ^{o}C.

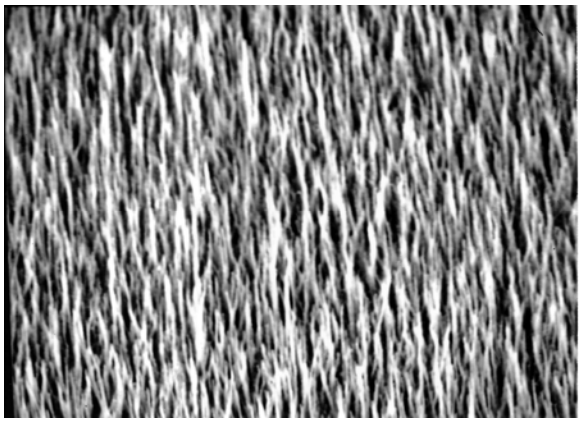

Original CNT sample

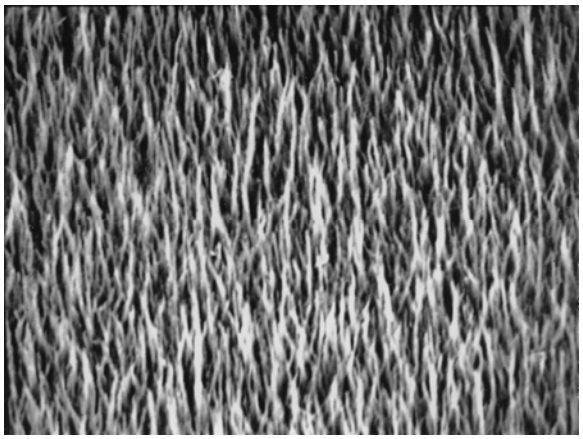

After heating at 800 ^{o}C for I hour

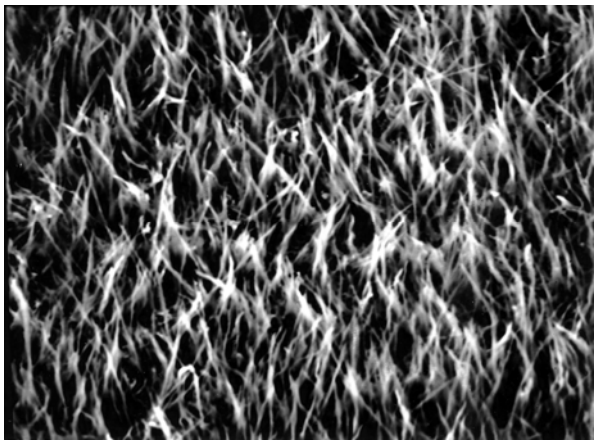

After heating at 1200 ^{o}C for I hour

Figure 42. SEM images of the originally CNTs and CNTs after thermal treatment

Furthermore the field emission properties of these thermally treated samples were characterized and compared to the original CNT sample. The field emission measurement results are shown in figure 43. As we can see from figure 43, the thermal treatment didn't alter the field emission properties of the CNT samples. The field emission of the CNT samples after thermal treatment had very similar emission characteristics as the original untreated sample. This was a very surprise finding, given the apparent morphology change observed on the sample treated at 1200 ^{o}C. However, this was also a welcoming

news as it indicated that the emission from CNTs were stable even after heated to a very high temperature.

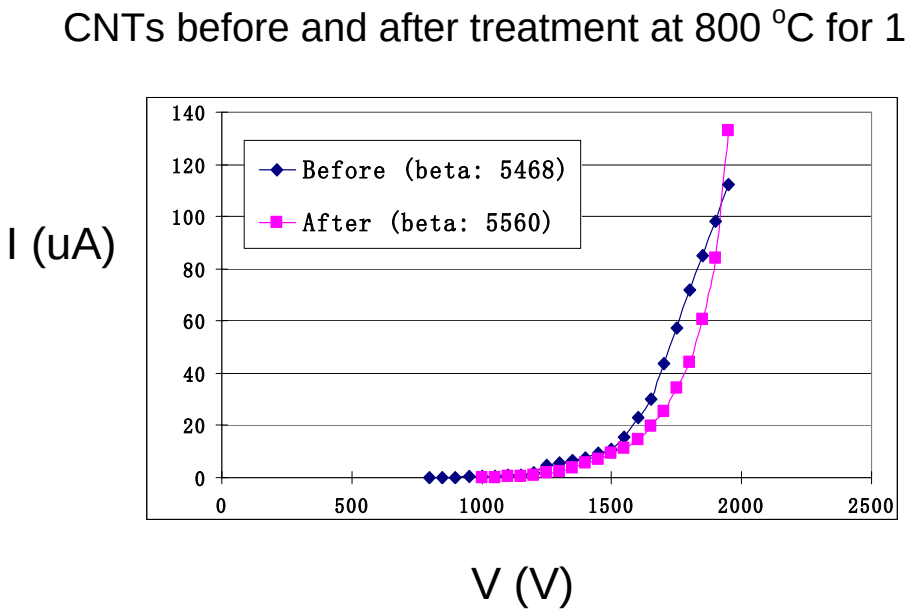

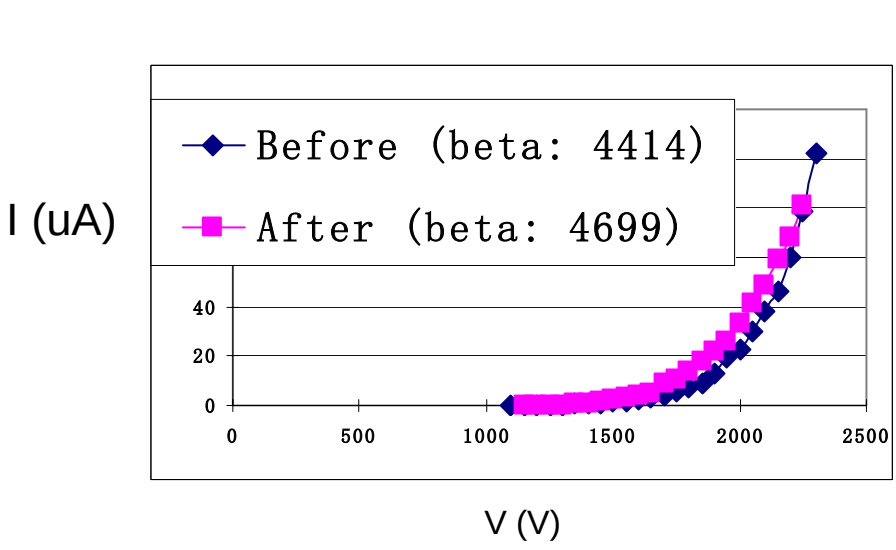

Figure 43. Field emission results of the CNT samples before and after thermal treatment.

Conclusions:

A highly efficient CNT based thermionic cathode was demonstrated. This cathode is capable of emitting electron at a current density two order of magnitude stronger then a typical fluorescent cathode at same temperatures, or capable of emitting at same current density but at temperature about 300 ^{o}C lower than that of a fluorescent cathode. Detailed fabrication techniques were developed including CVD growth of CNTs and sputter deposition of oxide thin films on CNTs. These are mature technologies that have been widely used in industry for large scale materials processing and device fabrications, thus, with further development work, the techniques developed in this project can be scaled-up in manufacturing environment. The prototype cathodes developed in this project were tested in lighting plasma discharge environment. In many cases, they not only lit and sustain the plasma, but also out perform the fluorescent cathodes in key parameters such like cathode fall voltages. More work will be needed to further evaluate more detailed and longer term performance of the prototype cathode in lighting plasma.

Appendix A: List of the publications under the project:

1) F. Jin, Y. Liu, C. M. Day, S. Little, "Enhanced field emission from carbon nanotubes with a thin layer of low work function barium strontium oxide surface coating," published in Journal of Vacuum Science & Technology B 25, 1785 (2007)

2) F. Jin, Y. Liu, S. Little, C. M. Day, "A new thermionic cathode based on carbon nanotubes with a thin layer of low work function barium strontium oxide surface coating," Proceedings of the 11th International Symposium on the Science and Technology of Light Sources, May, 2007.

3) F. Jin, Y. Liu, C. M. Day, S. Little, "Enhanced field emission from carbon nanotubes with a thin layer of low work function barium strontium oxide surface coating," also selected for the October 29, 2007 issue of Virtual Journal of Nanoscale Science & Technology.

4) Feng Jin, Yan Liu, Christopher Day, and Scott Little, "Enhanced Thermionic Emission from Barium Strontium Oxide Coated Carbon Nanotubes," Proceedings of the 8th IEEE International Vacuum Elelectronics Conference, May, 2007.

5) Feng Jin, Yan Liu and Christopher Day, "Barium strontium oxide coated carbon nanotubes as field emitters," Applied Physics Letters, April, 2007, Vol. 90 Issue 14.

6) Feng Jin, Yan Liu, Christopher Day and Scott Little, "Enhanced electron emission from functionalized carbon nanotubes with a barium strontium oxide coating produced by magnetron sputtering," Carbon, Mar 2007, Vol. 45 Issue 3, p587-593.

7) Yan Liu and Christopher Day, Scott Little and Feng Jin, "Thin film deposition of barium strontium oxide by rf magnetron sputtering," Journal of Vacuum Science & Technology A 24(6), Nov/Dec 2006.

8) Feng Jin, Yan Liu and Christopher Day, "Thermionic Emission from Carbon Nanotubes with a Thin Layer of Low Work Function Barium Strontium Oxide Surface Coating," Applied Physics Letters, 88, 163116 (2006).

9) Feng Jin and Chris Day, "A New Carbon Nanotube Based Field Enhanced Thermionic Cathode," Proc. MRS (Materials Research Society), HH13.33 (February, 2005).